Annales
Geophysicae

Polar, Cluster and SuperDARN evidence for high-latitude merging during southward IMF: temporal/spatial evolution

N. C. Maynard[1], **D. M. Ober**[1], **W. J. Burke**[2], **J. D. Scudder**[3], **M. Lester**[4], **M. Dunlop**[5], **J. A. Wild**[4], **A. Grocott**[4], **C. J. Farrugia**[6], **E. J. Lund**[6], **C. T. Russell**[7], **D. R. Weimer**[1], **K. D. Siebert**[1], **A. Balogh**[8], **M. Andre**[9], **and H. Rème**[10]

[1]Mission Research Corporation, Nashua, New Hampshire, USA

[2]Air Force Research Laboratory, Hanscom Air Force Base, Massachusetts, USA

[3]Department of Physics and Astronomy, University of Iowa, Iowa City, Iowa, USA

[4]University of Leicester, Leicester, UK

[5]Rutherford-Appleton Laboratory, Didcot, UK

[6]EOS, University of New Hampshire, Durham, New Hampshire, USA

[7]IGPP, UCLA, Los Angeles, California, USA

[8]Imperial College, London, UK

[9]Uppsala University, Upsalla, Sweden

[10]CESR, Toulouse, France

Abstract. Magnetic merging on the dayside magnetopause often occurs at high latitudes. Polar measured fluxes of accelerated ions and wave Poynting vectors while skimming the subsolar magnetopause. The measurements indicate that their source was located to the north of the spacecraft, well removed from expected component merging sites. This represents the first use of wave Poynting flux as a merging discriminator at the magnetopause. We argue that wave Poynting vectors, like accelerated particle fluxes and the Walén tests, are necessary, but not sufficient, conditions for identifying merging events. The Polar data are complemented with nearly simultaneous measurements from Cluster in the northern cusp, with correlated observations from the SuperDARN radar, to show that the locations and rates of merging vary. Magnetohydrodynamic (MHD) simulations are used to place the measurements into a global context. The MHD simulations confirm the existence of a high-latitude merging site and suggest that Polar and SuperDARN observed effects are attributable to both exhaust regions of a temporally varying X-line. A survey of 13 merging events places the location at high latitudes whenever the interplanetary magnetic field (IMF) clock angle is less than $\sim 150°$. While inferred high-latitude merging sites favor the antiparallel merging hypothesis, our data alone cannot exclude the possible existence of a guide field. Merging can even move away from equatorial latitudes when the IMF has a strong southward component. MHD simulations suggest that this happens when the dipole tilt angle increases or when IMF B_X increases the effective dipole tilt.

Key words. Magnetospheric physics (magnetopause, cusp and boundary layers; magnetospheric configuration and dynamics; solar wind-magnetosphere interactions)

Correspondence to: N. C. Maynard
(nmaynard@mrcnh.com)

1 Introduction

It is generally accepted that merging between the interplanetary magnetic field (IMF) and the Earth's magnetic field (Dungey, 1961) is the principal coupling mechanism for solar wind plasma entry to the magnetosphere. The nature, location, and temporal dependence of merging remain open questions. The purpose of this paper is to provide evidence that merging often proceeds away from the equator.

Accelerated flows of magnetosheath plasma observed near the subsolar magnetopause (near the Earth-Sun line) provide in situ evidence of the merging process (Paschmann et al., 1979; Sonnerup et al., 1981). Minimum variance analyses of magnetic field measurements were employed to show that the magnetopause acted as a rotational discontinuity with a finite B_{normal}, proportional to the merging rate. However, establishing an unambiguous finite B_{normal} can be difficult. Jump conditions across the discontinuity satisfy the Walén relationship, indicating that the change in the ion velocity is proportional to the change in the magnetic field. Observations of accelerated flows, often identified by "D-shaped" distributions in velocity space (Cowley, 1982), have been regarded as standard signatures of merging (e.g. Gosling et al., 1982; Paschmann et al., 1986; Sonnerup et al., 1990).

X-type merging configurations with oppositely directed field lines (Levy et al., 1964) were generalized by Sonnerup (1974) to include merging between the antiparallel components of **B**, along a line that hinges about the subsolar point (Gonzales and Mozer, 1974). Crooker (1979) offered an alternate hypothesis in which merging occurs wherever magnetospheric and magnetosheath field lines are aligned antiparallel to each other. For most IMF orientations the antiparallel location is at high latitudes on the magnetopause. By high (low) latitudes, we mean in the general vicinity of the cusp (equator). Both hypotheses locate merging at the poleward

boundary of the dayside cusp during periods of purely northward IMF. Merging has been definitively identified there by Scudder et al. (2002a).

One difficulty in locating the merging line relates to a lack of accelerated particles observed during magnetopause crossings. In fact, decelerated flows are encountered in the boundary layer (Eastman et al., 1976). Aggson et al. (1983) transformed electric fields measured by ISEE-1 at the magnetopause into a de Hoffman-Teller (H-T) reference frame (de Hoffman and Teller, 1950). Data measured by Polar were subjected to a Galilean transformation to a reference frame moving with a velocity V_{HT}. In this reference frame the electric field component perpendicular to the magnetic field transforms to zero. H-T reference frames exist for rotational but not for most tangential discontinuities. The transformation will not remove the electric field internal in the layer in a tangential discontinuity (e.g. Lee and Kan, 1979). Thus, the identification of a H-T frame for ordering satellite measurements that holds internally in the current layer implies the traversal of a rotational discontinuity. In the H-T frame the plasma velocity is directed along the magnetic field and is equal to the local Alfvén speed.

While increased velocities were observed during some ISEE-1 magnetopause crossings, Aggson et al. (1984) also reported decelerated flows. Moreover, they emanated from a merging site poleward of the satellite. Scudder (1984) calculated that, as the merging site moved off the equator, the exhaust velocity from the X-line should equal the sum from the merging acceleration and the local magnetosheath velocity at the merging site. Hence, the outflow velocity in inertial space may be significantly less than the Alfvén speed. In a recent analysis of 69 magnetopause crossings, Phan et al. (1996) found that, of the 42 that "satisfied" the Walén test, 21 had velocity changes that produced normalized slopes on the average of 0.6, which is less than unity predicted from a single component merging X-line. They concluded that (1) merging sometimes occurs at latitudes higher than the satellite and (2) earlier studies that restricted merging sites to only equatorial latitudes were biased to include only those events with significant acceleration (e.g. Scurry et al., 1994). Scudder et al. (1999) showed that the Walèn test was better performed with electrons whenever currents were present. Under these conditions, the normalized slopes for the ion Walén test detected during the same crossings were often significantly less than 1, which does not match expectations. They showed that during many of these non-conforming crossings, the normalized slopes of the electrons were consistently near $+/-1$, as needed for a conclusive rotational discontinuity test.

In a recent study Maynard et al. (2001b) correlated rocket measurements of electric fields near the Northern-Hemisphere cusp with geoeffective interplanetary electric fields (IEF) measured upstream in the solar wind by the Wind satellite. They found that observed lag times were significantly less than those predicted for simple advection. The IMF was dominated by B_X and the clock angle in the $Y - Z$ plane was near $90°$. The short lag time and the dominant B_X forced consideration of tilted phase planes of the IEF and

placed the location of merging at high latitudes in the Southern Hemisphere. Whether merging followed the antiparallel hypothesis of Crooker (1979) or whether a small guide field was present could not be ascertained with the available data. Either way, a portion of the cusp in the Northern Hemisphere was responding to a merging source in the Southern Hemisphere. Within the same all-sky picture of the dayside cusp taken at Ny-Ålesund, responses to high-latitude merging in the Northern Hemisphere were also identified. Because of IMF B_Y, the cusp was bifurcated into source regions originating from high-latitude merging in the Northern and Southern Hemispheres, while IMF B_X controlled the timing of the interactions in each hemisphere. Merging rates responded to small-scale variations of the IEF, as evidenced by electric fields observed at the rocket and by 557.7 nm emissions captured in the all-sky images. Because of the strong B_X, the lag time was 14 min longer for the Northern Hemisphere merging site compared to the Southern Hemisphere site. The bifurcation of the cusp with B_Y and the need for antiparallel reconnection under those conditions was also deduced by Coleman et al. (2001).

Weimer et al. (2002) utilized data from four satellites in the solar wind to show that lag times varied continuously and to construct the phase plane in an over-determined way. They demonstrated that the orientations of IEF phase planes change significantly on time scales of tens of minutes, and that the small-scale variations often remained coherent while propagating over 200 R_E in the solar wind. Both factors were used by Maynard et al. (2001b) to reach the interpretation described above. Variable lag times from the shifting orientation of the phase plane of the IEF must be considered in any assessment of IMF influences on merging processes. Lag times do not, in general, remain constant.

Projections of the dayside cusp onto the ionosphere may be quite wide (Maynard et al., 1997). Plate 1 of Maynard et al. (2001b) indicates that signatures of high-latitude merging in the local hemisphere may be significantly displaced from noon when IMF B_Y is large. Azimuthal plasma velocity enhancements may be expected from the merging and subsequent $\mathbf{J} \times \mathbf{B}$ acceleration.

Cowley (1982) documented the ion signatures expected in the vicinity of rotational discontinuities that attend X-type merging lines. Near the outer separatrix, transmitted or accelerated magnetospheric ions may be found, along with accelerated and incident magnetosheath ions. Near the inner separatrix, the incident or cold distribution is of magnetospheric origin, while accelerated distributions from magnetosheath sources may also be observed. Distribution-function isocontours in $v_{||}-v_{\perp}$ phase space exhibit "D" shapes when acceleration has occurred. Finding a "D" shaped isocontour displaced from the origin has been cited by Fuselier et al. (1991) as "strong evidence" that reconnection has occurred. Bauer et al. (2001) reported many magnetopause crossings that "satisfied" Walén tests using ion velocities but lacked clear "D"-shaped distributions. They attributed the missing "D" to pattern blurring by mirroring particles. By itself, a "D" shaped distribution is a necessary but not a

sufficient signature of merging, since ambipolar parallel electric fields associated with electron pressure gradients can accelerate ions without merging (Scudder et al., 2002b).

A second signature of merging may be identified from wave Poynting fluxes $(\Delta \mathbf{E} \times \Delta \mathbf{B})/\mu_0$, where $\Delta \mathbf{E}$ and $\Delta \mathbf{B}$ are the fluctuations as described below. When merging occurs, Alfvén waves are launched to communicate information to magnetically connected regions (Atkinson, 1992). The associated wave Poynting vector is directed away from the source since it represents escaping electromagnetic energy. This electromagnetic energy flux should be strongest along the separatrices. Again, this is a necessary but not sufficient condition for identifying merging events, since other mechanisms can generate Alfvén waves that carry parallel Poynting flux.

Geotail was the first satellite to skim along the magnetopause, while moving parallel to the equatorial plane. During multiple crossings, Nakamura et al. (1998) observed increased speeds accompanied by ion heating and inferred them to have come from distant merging sites. More recently, Kim et al. (2002) observed accelerated flows at the magnetopause near the subsolar equator. They interpreted changes in direction as evidence for component merging, with the separator moving north and south relative to the spacecraft. Phan et al. (2000) used Geotail and Equator S measurements on the dawn flank of the magnetopause to provide nearly simultaneous observations of bi-directional flows from an X-line between the spacecraft in the equatorial region. This was for a nearly pure B_Z south condition.

In the 2000–2002 period, the $9\,R_E$ apogee for the Polar satellite orbit has been close to the equator. On many days it spent long periods skimming along the magnetopause from south to north, roughly at quadrature to the Geotail orbital plane. Often the satellite either traversed the magnetopause very slowly, or failed to cross it completely. Thus, temporal variations may be clearly identified, but spatial scales are not as easily determined. If current layers are crossed slowly and merging occurs at high latitudes, one should not assume that observations of an inner separatrix near the equatorial plane will be followed by an observation of an outer separatrix. With the merging line located far from the spacecraft it is probable that only one separatrix will be observed. Merging may vary both temporally and spatially, occurring simultaneously at multiple sites. High-latitude merging is expected to be more temporally variable, since an X-line will not be intrinsically stable when the tangential magnetosheath flow is super-Alfvénic (Cowley and Owen, 1989; Rodger et al., 2001).

Evidence that merging proceeds away from the equator plane at high latitudes is seen in a number of the Polar skimming passes. In the following sections, we present time-varying observations from Polar, Cluster and SuperDARN acquired on 12 March 2002, to establish the temporal and spatial variability of the merging process. Using other events and comparisons to simulation results, we extend these observations to show that high-latitude merging is more com-

mon than generally thought when the clock angle is less than 150° and may occur at even greater clock angles.

2 Measurements

Several Polar instruments contribute to this study. The Hydra Duo Deca Ion Electron Spectrometer (DDIES) (Scudder et al., 1995) consists of six pairs of electrostatic analyzers looking in different directions to acquire high-resolution energy spectra and pitch-angle information. Full three-dimensional distributions of electrons between 1 eV and 10 keV and ion fluxes with an energy per charge ratio of $10\,\mathrm{eV\,q^{-1}}$ to $10\,\mathrm{keV\,q^{-1}}$ were sampled every 13.8 s. The electric field instrument (EFI) (Harvey et al., 1995) uses a biased double probe technique to measure vector electric fields from potential differences between 3 orthogonal pairs of spherical sensors. In this paper we present measurements from the long wire antennas in the satellite's spin plane. The Magnetic Field Experiment (MFE) (Russell et al., 1995) consists of two orthogonal tri-axial fluxgate magnetometers mounted on nonconducting booms. Electric and magnetic fields were sampled at a rate of $16\,s^{-1}$. Most of the presented data were spin averaged using least-squares fitting to sine waves.

The Advanced Composition Explorer (ACE) spacecraft is located in a halo orbit around L_1 in front of the Earth to monitor interplanetary conditions. The solar wind velocity was measured by the Solar Wind Electron, Proton, and Alpha Monitor (SWEPAM) (McComas et al., 1998). A tri-axial fluxgate magnetometer measured the vector interplanetary magnetic field (Smith et al., 1998). We also use data from the Magnetic Field Investigation (Lepping et al., 1995) and the Solar Wind Experiment (Ogilvie et al., 1995) on Wind for cross-checks. Wind was executing a distant prograde orbit; hence, it generally had large Y coordinates in this interval.

On one of the studied days the 4 Cluster spacecraft passed through the cusp while Polar was skimming the magnetopause. Magnetic field measurements were made on each of the Cluster spacecraft by tri-axial fluxgate magnetometers (Balogh et al., 2001).

In addition to the measurements of the vector magnetic field, the configuration of the 4 Cluster spacecraft allowed estimates of $\nabla \times \mathbf{B}$ to determine local current flows. The nominal separation distances between the s pacecraft at this time was $\sim 600\,\mathrm{km}$. The electric field and wave instrument (EFW) monitored both electric field components in the ecliptic plane using biased double probes (Gustafsson et al., 1997). The Cluster Ion Spectrometer (CIS) experiment provided 3-D ion distributions with mass per unit charge composition using the Composition and Distribution Function (CODIF) analyzer (Rème et al., 1997). Ion measurements are available only from spacecraft 1, 3, and 4.

In addition to the satellite measurements, the Super-DARN coherent backscatter radar network provided information about ion convection in the high-latitude ionosphere over a wide range of local times (Greenwald et al., 1995). Single-component drift measurements from each of the radar
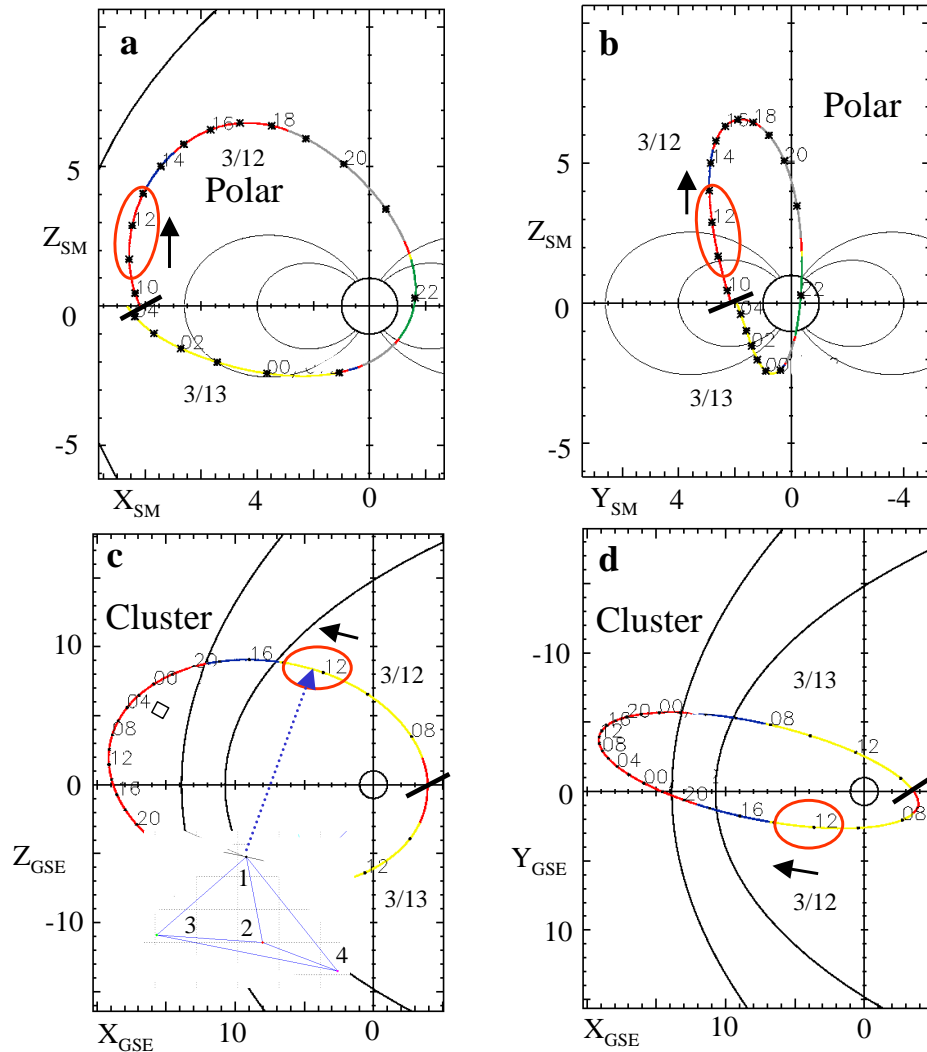
Fig. 1. Plots of the Polar orbit in the XZ and YZ solar magnetospheric (SM)coordinate planes and of the Cluster orbit in the XZ and XY geocentric solar ecliptic (GSE) planes for the 12 March 2001 event. The regions of interest are highlighted by the red ovals. The black line across the orbit track in each plot notes the start of the orbit trace. Nominal magnetopause and bow-shock configurations are indicted in panels a, c and d as appropriate. The circles at the origin represent the Earth. In panel c the insert shows the configuration of the 4 Cluster spacecraft, with Cluster 3 leading and Cluster 4 trailing. The tetrahedron configuration is maintained quite well during the interval of interest. Spacecraft separation is of the order of 600 km.

sites were iterated with an empirical model to estimate 2-dimensional vector drifts (Ruohoniemi and Baker, 1998).

3   Analysis methods

Our analysis concerns large-scale aspects of coupling between the IMF and the magnetosphere-ionosphere system, from global- to meso-scale perspectives, where electron gyrotropy applies and merging actually occurs (Scudder et al., 2002a). We do not consider the microphysics of the merging process. Addressing problems with simultaneous observations from diverse locations properly constrains our interpretations. Analyzing Polar skimming passes presents challenges and advantages. Since the magnetopause expands and contracts with changing solar wind conditions, multiple

crossings often occur. Polar sometimes remains in the vicinity of the magnetopause for hours. While this reduces our present knowledge about spatial structuring, it allows us to follow temporal responses to changes in the IMF and solar wind dynamic pressure, and thereby establish close correlations with external drivers. We correlate observed behaviors with temporal variations in other regions, such as in the ionosphere as measured by SuperDARN, or in the outer cusp as measured by Cluster.

Interpretations of satellite measurements were tested for reasonableness through comparisons with predictions of simulations using the Integrated Space Weather Model (ISM). ISM is a large-scale magneto-hydrodynamic (MHD) code developed by Mission Research Corporation to simulate the magnetosphere-ionosphere system from its front boundary
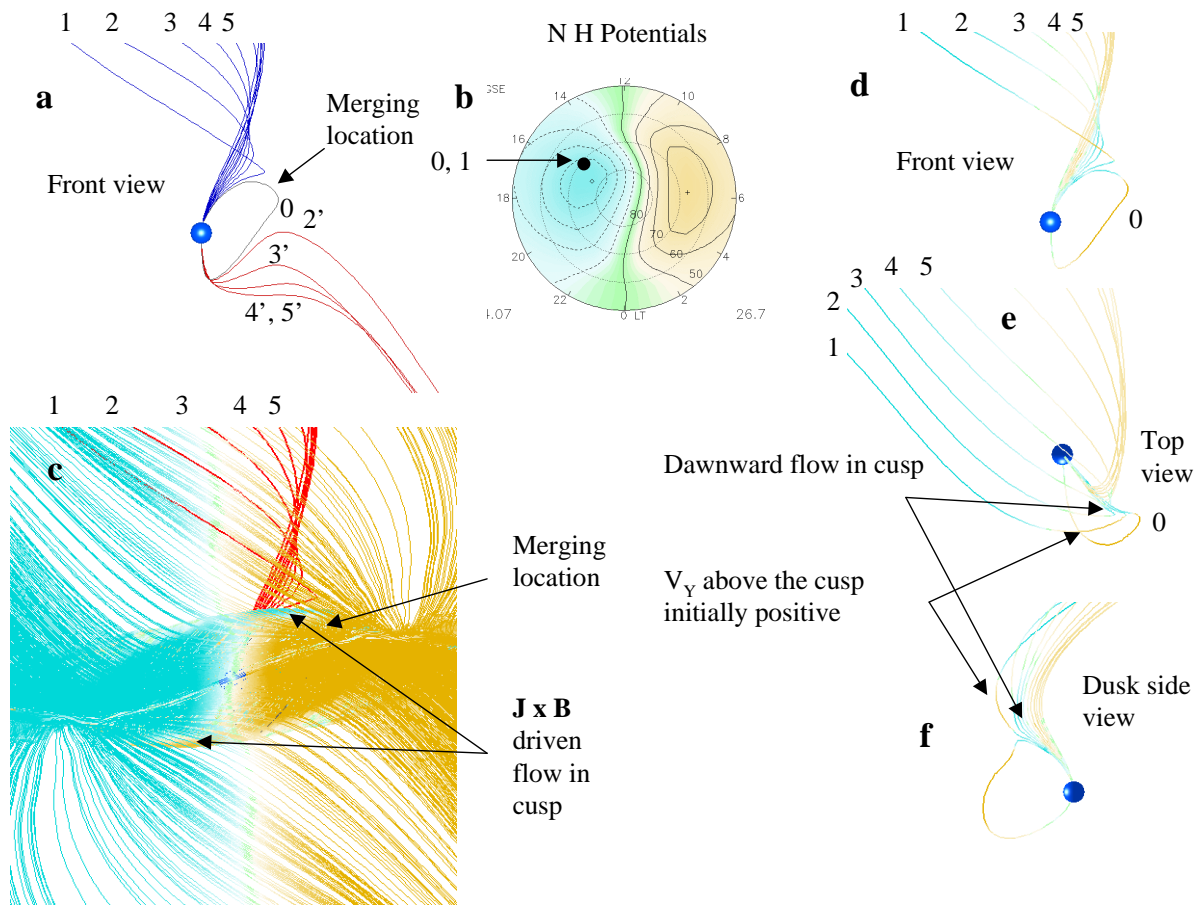
Fig. 2. Traced magnetic field lines from a MHD simulation using the Integrated Space Weather Model (ISM). Figure 2a shows a set of field lines flowing away from a high-latitude merging site. Trace 0 is closed, and its origin in the Northern Hemisphere is shown in Fig. 2b to be between 15 and 16 MLT and 71° latitude. All others are open. Figures 2d–f show three views of these same field lines colored with the Y component of the velocity. Figure 2c shows the complete set of first-open field lines traced from the ionosphere in each hemisphere and also colored with V_Y (see text).

40 R_E upstream in the solar wind, to the base of the iono-sphere near the Earth, and to deep in the magnetotail (White et al., 2001). Lacking the microphysics and resolution needed to accurately portray merging, ISM accomplishes the process through dissipation, either explicitly introduced by current dependent resistivity, or introduced by the code through the partial donor method (PDM) of Hain (1987), to maintain stability in the presence of steep gradients (see White et al., 2001, for more details). Through simulations of steady-state conditions or of responses to step-function driver variations, cause and effect relationships are easily iso-lated. This approach was used successfully by Maynard et al. (2001a; 2003a), to establish the sash (originally identi-fied in the simulations by White et al., 1998) as a reconnec-tion site, and to provide an explanation for short-lived, sun-aligned arcs emanating from the high-latitude open-closed boundary of the nightside auroral oval. Synergism between data analysis and the simulations provides a powerful tool for understanding the complex interactions of the solar wind with the magnetosphere-ionosphere system.

Polar often fails to traverse the magnetopause current layer

completely. Hence, we use two markers to identify occur-rences of merging. The first is to demonstrate the presence of accelerated parallel ion fluxes. Guidance comes from the interpretation of distribution functions given by Cowley (1982). Our second marker is the presence of parallel Poynt-ing flux. Active merging must be communicated away from the site to other regions along the magnetic field lines by Alfvén waves. Parallel Poynting flux, carried by waves prop-agating away from a source, can indicate where active merg-ing is proceeding. Whereas the dc Poynting flux specifies the transport of energy by convective flow, the wave Poynt-ing flux, determined from $\Delta\mathbf{E} \times \Delta\mathbf{B}$, measures energy flow carried by Alfvén waves. To calculate the wave Poynting flux we subtract the average magnetic field (B_0) and elec-tric field (E_0), determined using a sliding boxcar average of 3 min, from the measured field quantities. The above cross product is then taken. When the sharp changes in **B** occur as the magnetopause current layer is traversed, boxcar averages can allow variations from large-scale changes to contaminate the results. To avoid this problem we terminate the wave Poynting flux calculation at the edge of the current layer
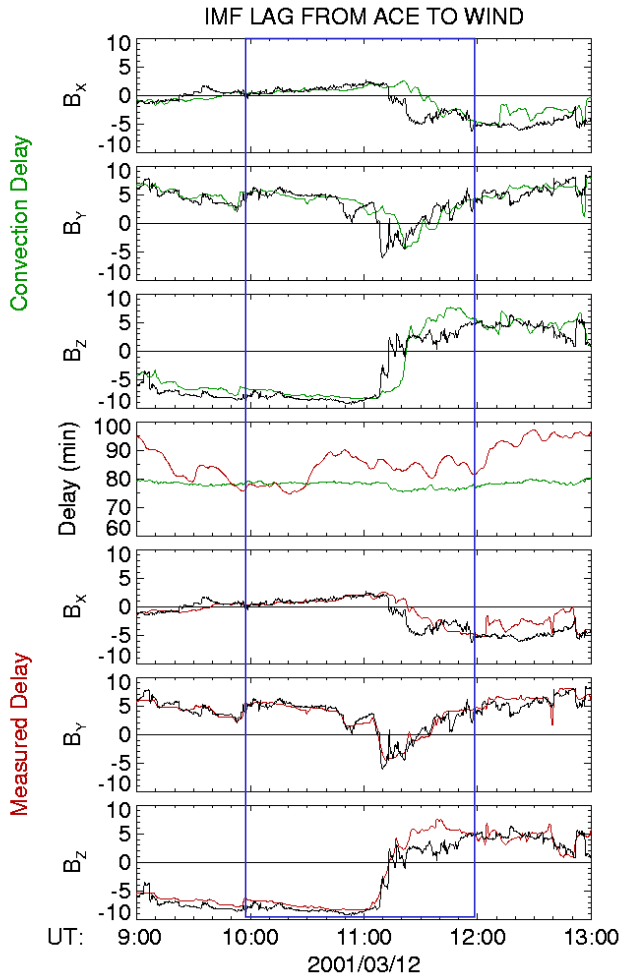
Fig. 3. Comparison of IMF data from ACE and Wind for 12 March 2001. **(a)–(c)** The comparison is made using the advection time (plotted in the green trace in panel **(d)**. **(e)–(g)** The comparison is made using the variable lag time, calculated using the technique of Weimer et al. (2002) and shown by the red trace in panel (d). The region of particular interest is highlighted by the blue box. Note that the lag time is increasing prior to 10:40 UT, then levels off, and later decreases as the directional discontinuity is approached near 11:00 UT.

and resume the calculation when the major change in B has been completed. Calculations using spin-averaged data have a resolution of 6 s on Polar and 4 s on Cluster. Since there are other ways to generate Alfvén waves, we look for the temporal concurrence of accelerated ions and parallel Poynting flux, coming from the same direction, as the signatures of merging and indicators of its location with respect to the spacecraft.

To aid interpretation we establish the variable lag times for IMF features between ACE and Polar. The tilts of phase planes in the solar wind can change on short time scales (Maynard et al., 2001b; Weimer et al., 2002). The proper lags from ACE to Polar are adjusted by requiring that the IMF clock angle in the $Y - Z$ plane be maintained across the bow-shock (Song et al., 1992). Whenever Polar is in the
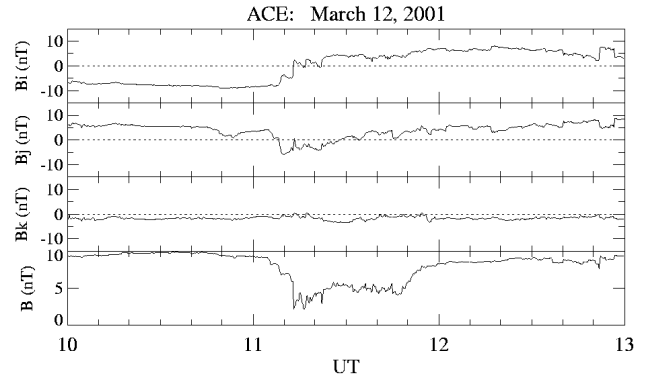

Fig. 4. ACE magnetic field data between 10:00 and 13:00 UT in minimum variance coordinates, where i is the direction of maximum variance and k is the direction of minimum variance.

magnetosheath, this technique can be used. When Polar is in the boundary layer or cusp, we must rely on the availability of at least two satellites in the solar wind, to apply the technique described by Weimer et al. (2002) and to determine how lag times change.

Wherever possible we look for corroborating data from diverse sites, such as SuperDARN or DMSP satellites in the ionosphere and/or Cluster in the cusp. An example in which data from all three sources can be utilized comes from the 11:00 to 13:00 UT interval on 12 March 2001.

4   Observations from 12 March 2001

4.1   Overview

On 12 March 2001, the Polar orbit skimmed the subsolar magnetopause while Cluster passed through the Northern Hemisphere cusp. Figures 1a and b show the $X - Z$ and $Y - Z$ solar magnetospheric (SM) projections of the Polar orbit. Arrows indicate the direction of spacecraft motion. The region of interest lies inside the red ovals. Polar crossed it between 11:00 and 13:00 UT. At 12:00 UT the dipole was tilted tailward 0.3°. Hence, the subsolar point is very close to the X_{SM} axis. Figures 1c and d present the $X - Z$ and $X - Y$ projections of the Cluster orbits in GSE coordinates. Cluster crossed from the lobe to the magnetosheath above the cusp between 12:00 and 12:30 UT. Red ovals mark the period of interest. The insert in Fig. 1c depicts the tetrahedral configuration of the Cluster satellites at 12:00 UT. Cluster 3 is in front, while Cluster 4 trails the other three. All spacecraft were located slightly post-noon. In addition, SuperDARN radar provided estimates of the ionospheric convection patterns. Thus, we can trace ionospheric responses to activity in the high-altitude cusp and on the dayside magnetopause, and from there to its sources in the solar wind.

Figure 2 provides a conceptual context for measurements acquired in the various regions. Traced field lines come from an ISM simulation using an IMF clock angle of 135°, similar to the angle of 140° for the 12 March magnetopause cross-
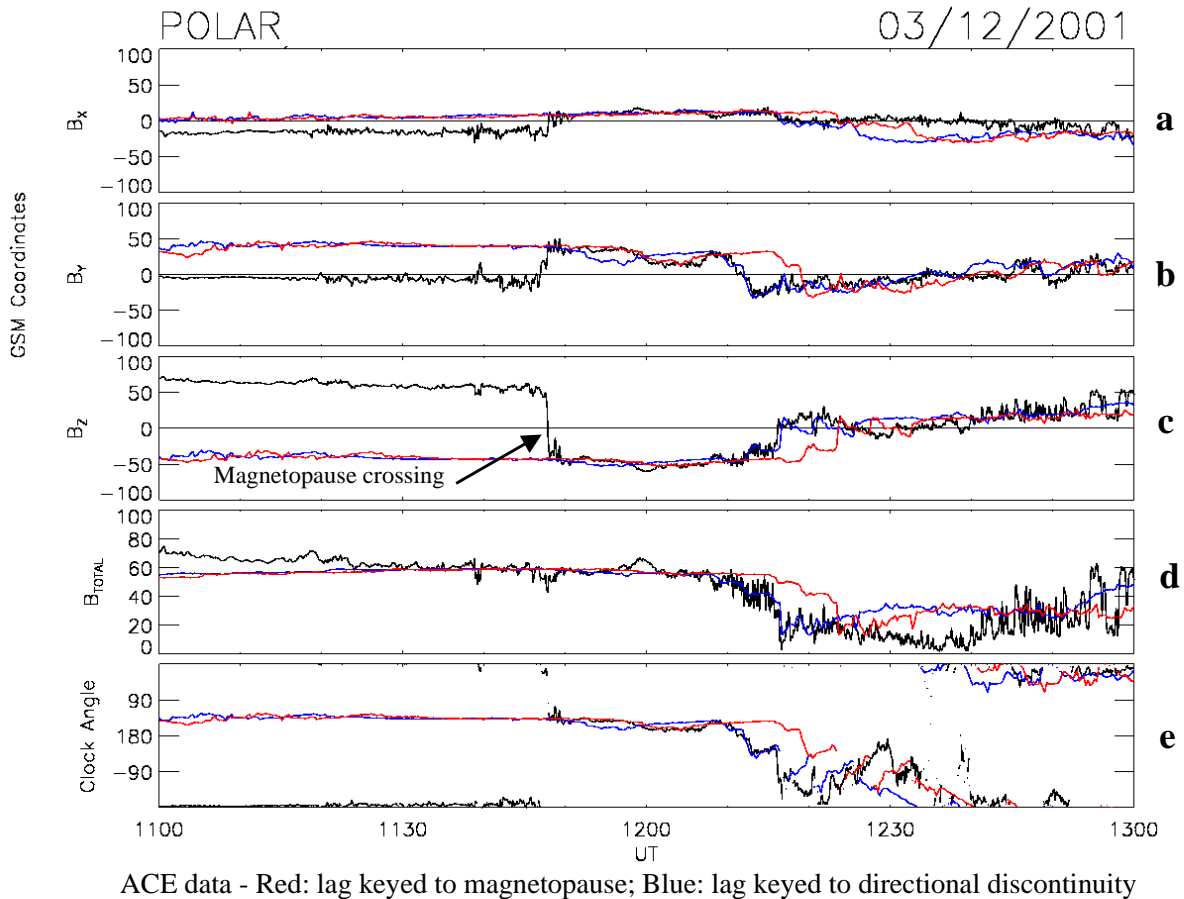
Fig. 5. Comparisons of the components, magnitude and clock angle of the magnetic fields measured at ACE (red and blue) and at Polar (black). The lag time is set at 70.5 min for the red ACE traces, which is appropriate for the magnetopause crossing observed at 11:48 UT and the next 15 min. A lag time of 63.5 min (blue ACE traces) was used to bring into alignment the region around the directional discontinuities. The scale for ACE data is one-sixth of that marked.

ing. Last-closed field lines were found starting from the ionosphere in each hemisphere. By moving poleward 10 km in the ionosphere from the trace point of each closed field line, we define a set of "first" open field lines. The last-closed and first-open field lines are labeled 0 and 1 in Fig. 2a. They map from the black dot in the potential pattern in Fig. 2b, near 15 MLT and 71° magnetic latitude, and pass through the post-noon cusp. Field-line 0 also traverses the low-latitude region of the post-noon magnetopause. The closed field line maps to near the zero equipotential line between the two convection cells in the Southern Hemisphere.

To understand how the field lines change after merging, we have traced a number of field lines from a series of points along the Northern Hemisphere equipotential that passes through the origin of trace 0. The first 4 of these, labeled 2–5 in Fig. 2a, show how a field line evolves as it is dragged back over the magnetopause. A similar set of field lines was mapped from the equipotential contour in the Southern Hemisphere at the end of trace 0 and is labeled 2'–5'. Line 2' probably pairs best with 2, although there is no way to trace the evolution of exact pairs from a merging site. A high-latitude merging site can be inferred to be located close to

where line 1 bends. Subsequent field lines show how they unbend and traverse back through the cusp, as they are dragged antisunward by the solar wind.

Figure 2c shows the complete set of first-open field lines traced from each hemisphere. The field lines are colored according to V_Y. The Northern Hemisphere set of field lines in Fig. 2a are colored red in Fig. 2c to show their position relative to the first-open field lines. The arrow points to the approximate locations of merging. Sharp bends in open field lines from the Northern Hemisphere indicate the general locations where merging is occurring. Most pre-noon (post-noon) field lines have a negative (positive) V_Y. Exceptions to this are in the cusp, where $\mathbf{J} \times \mathbf{B}$ forces from the currents associated with the curvature of newly-merged field lines to drive the flow westward (eastward) in the Northern (Southern) Hemisphere (Siscoe et al., 2000). Note that the velocity separator is not the merging separator. The more vertical velocity separator results when the merging $\mathbf{J} \times \mathbf{B}$ forces overcome the normal hydrodynamic flow away from the nose. A faint line at about a 20° tilt from the equator separates open field lines traced from the Northern Hemisphere from those traced from the Southern Hemisphere. The curvature of the
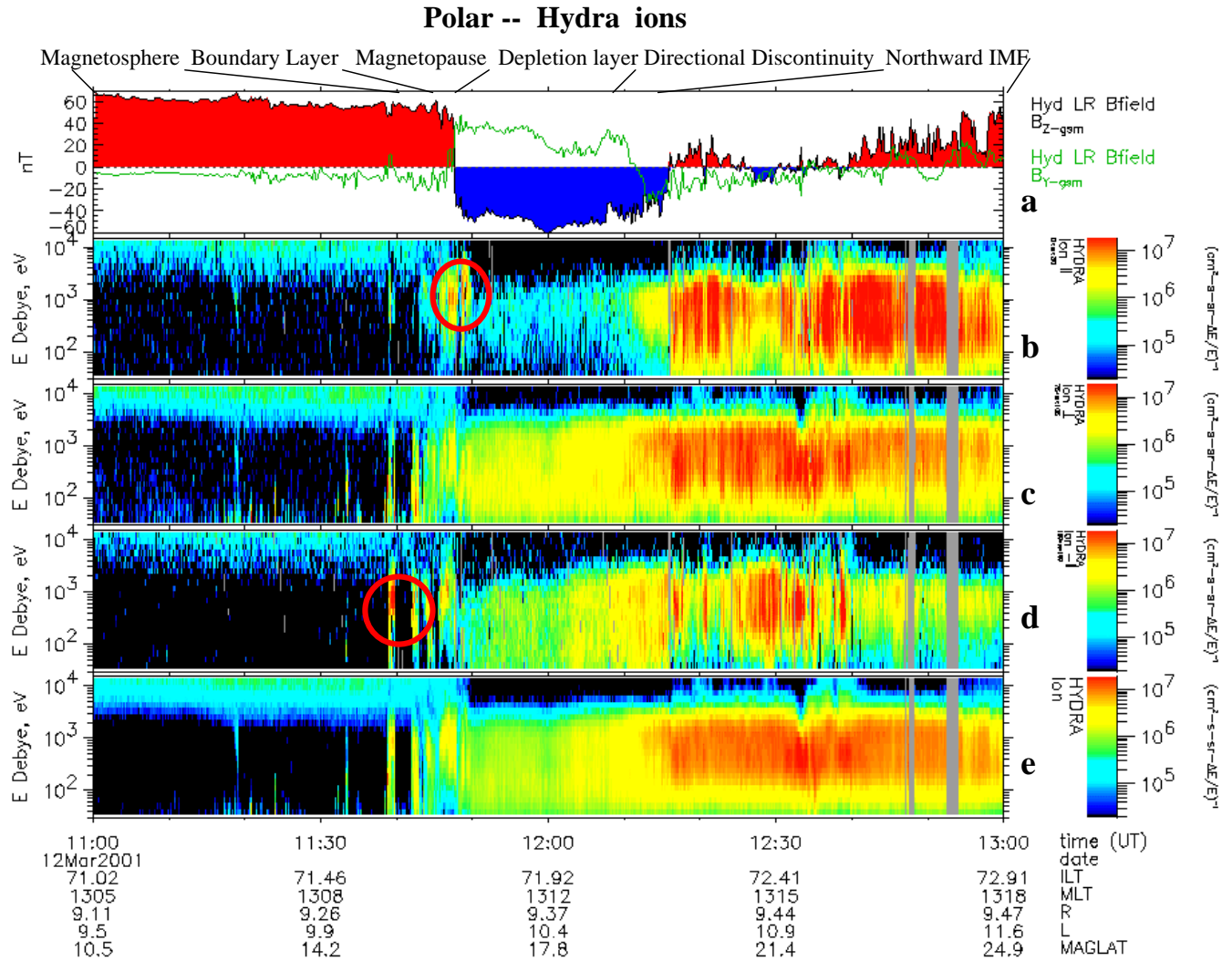
Polar -- Hydra ions

Fig. 6. Ion spectrograms and the magnetic field measured by Polar and plotted for the interval between 11:00 and 13:00 on 12 March 2001. **(a)** B_Z is shaded red (blue) for positive (negative) values. **(b)–(e)** Parallel, perpendicular, antiparallel and total ion energy spectra measured by the Hydra instrument. The circles highlight parallel or antiparallel accelerated ion fluxes associated with a contact and a crossing of the magnetopause.

field lines in the upper left indicate that most are pulling away from high-latitude merging sites in the Southern Hemisphere. The fact that the velocity separator is so much different from the separation of traced field lines is further evidence that low-latitude component merging is not a dominant process in the simulation. Figures 2d–f display the front, top, and side views of the Northern Hemisphere's closed and open field lines in Fig. 2a, colored with V_Y. Plasma flow in the boundary layer on the closed field line (0) is toward dusk. Flow above (in) the cusp on line 1 is toward dusk (dawn). Subsequently, the flow is toward dawn, both above and in the cusp, as the field line is dragged back through the mantle.

The primary flow direction near the magnetopause and in the outer portion of the boundary layer is determined by the diversion of flow from pressure gradients away from the stagnation region. Cowley and Owen (1989) have provided a

model of the flow, which combines the effects of the hydrodynamic diversion of flow from a stagnation point with the magnetic tension effects from merging. Siscoe et al. (2002) argue that the stagnation point should, in fact, be a stagnation line along the magnetic field line that passes through the nominal stagnation point at the nose.

Thus, ISM suggests that with merging at high latitudes in the Northern Hemisphere, Polar should observe flow away from noon at its post-noon location. In the post-noon cusp, the open boundary layer can maintain movement toward dusk, corresponding to the flow in the magnetosheath. Due to merging, the outer separatrix should initially continue to move toward dusk (applicable to Cluster as it passes through the magnetopause above the cusp), while the inner separatrix (as well as the foot of the field line) is pulled toward dawn.

4.2 Interplanetary conditions

IMF measurements were made by the Wind and ACE spacecraft located near $(-37, -165, 8)$ and $(227, -38, 4)$ R_E, respectively. Figures 3a–c show the three IMF components observed at the locations of the two spacecraft. Data are referenced to the UT of ACE measurements. Wind data (green) were lagged according to advection times based on the solar wind velocities measured at ACE (plotted as the green trace in Fig. 3d). The agreement between the traces in Figs. 3a–c is only moderate. This is especially evident beyond 10:00 UT. However, Weimer et al. (2002) showed that agreement could be improved by allowing for the lag time to vary on a minute-by-minute basis. Figures 3e–g show the same data (Wind data is colored red) using the calculated variable lag, which is plotted as the red trace in Fig. 3d. The variable lag reflects constantly changing tilts of IEF phase planes.

Our analysis focuses on the interval 10:00–12:00 UT. This interval is dominated by a large decrease in magnetic field strength between 11:12 to 11:50 UT (magnetic hole), shown in Fig. 4. A directional discontinuity occurs, probably rotational, during which GSM B_Y goes from positive to negative, and at 11:08 UT B_Z becomes less negative, preceding the sharp drop in B and reversal of B_Z by a few minutes. The combined structure bears resemblance to a configuration observed in the interplanetary medium in front of a magnetic cloud on 24 December 1996, by Farrugia et al. (2001). The magnetic field decrease was interpreted as a slow shock, which, coupled with the preceding rotational discontinuity, could be the signature of an upstream reconnection layer. The structure at ACE is approximately planar. Minimum variance analysis of the 3-h interval found a well-defined maximum variance plane with a normal component of -1.64 ± 0.66, consistent with the reconnection interpretation advanced by Farrugia et al. (2001) for the 24 December 1996 event. Figure 4 displays the three components and magnitude in principal axis coordinates. Polar observations at the magnetopause were acquired before and near the directional-discontinuity passage.

4.3 Polar observations

Polar encountered the magnetopause current layer several times before crossing the magnetopause at 11:48 UT. Variable lags help to establish the applicable solar wind conditions at that time. Figure 5 compares the three components and magnitude of **B**, along with clock-angle measurements at ACE and Polar during the interval from 11:00 to 13:00 UT. Plot scales were adjusted to reflect the factor of 6 increase after traversing the bow-shock. The ACE data were lagged by 70.5 min (red traces). The lag was determined by best matching the Polar and ACE clock angles between 11:50 and 12:05 UT. Note that it is different from the lag between ACE and Wind, displayed in Fig. 3, because of the different locations. This lag is good through 12:08 UT, when the first of the two directional discontinuities seen in the ACE and Wind data were sampled by Polar in the magnetosheath.
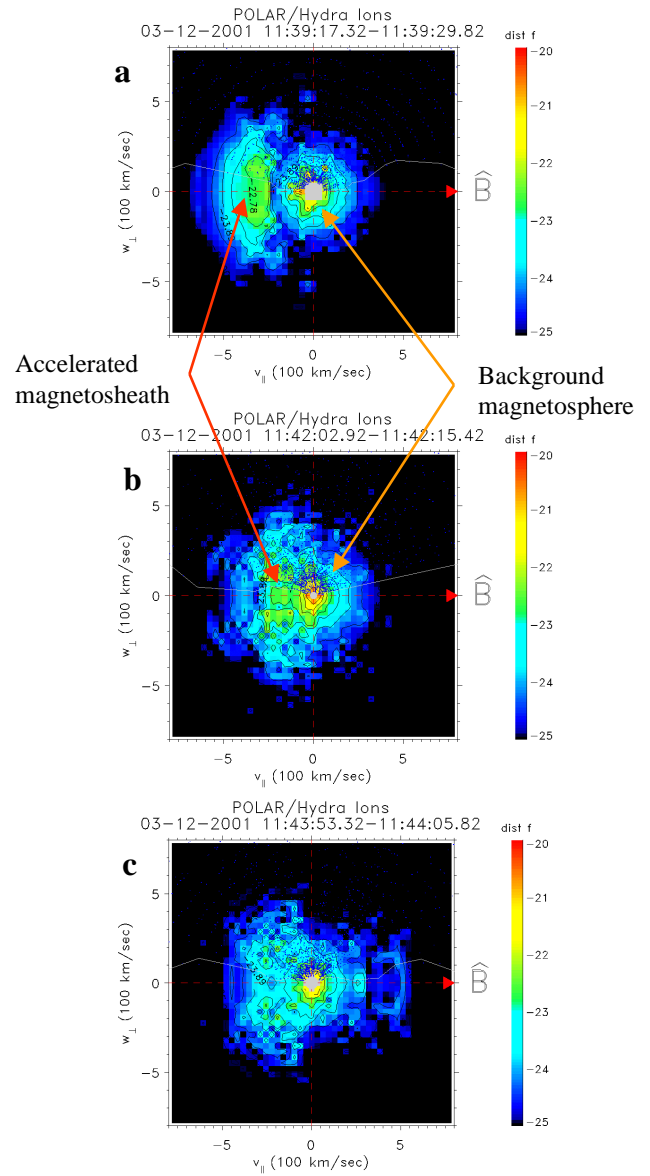

Fig. 7. Ion distribution plots for the interval of first contact with the magnetopause indicated by the first circle in Fig. 5.

The lag time decreased as the directional discontinuity structures approached. The variable lag time shown in Fig. 3d between ACE and Wind also was decreasing before the time of that structure, apparently due to the changed B_X. In Fig. 5 the blue traces represent the ACE data with a 63.5-min delay, which is more appropriate for times at the arrival of the directional discontinuities. The decreased lag significantly improves the fit between 12:10 and 12:18 UT. The fit in the center of the magnetic hole has further variations in lag. The directional discontinuities have similar normals to those determined at ACE and at Wind, showing that they have maintained coherence while passing through the bow-shock. Farrugia et al. (1991) found that the planarity is maintained in the magnetosheath but the orientation may change somewhat
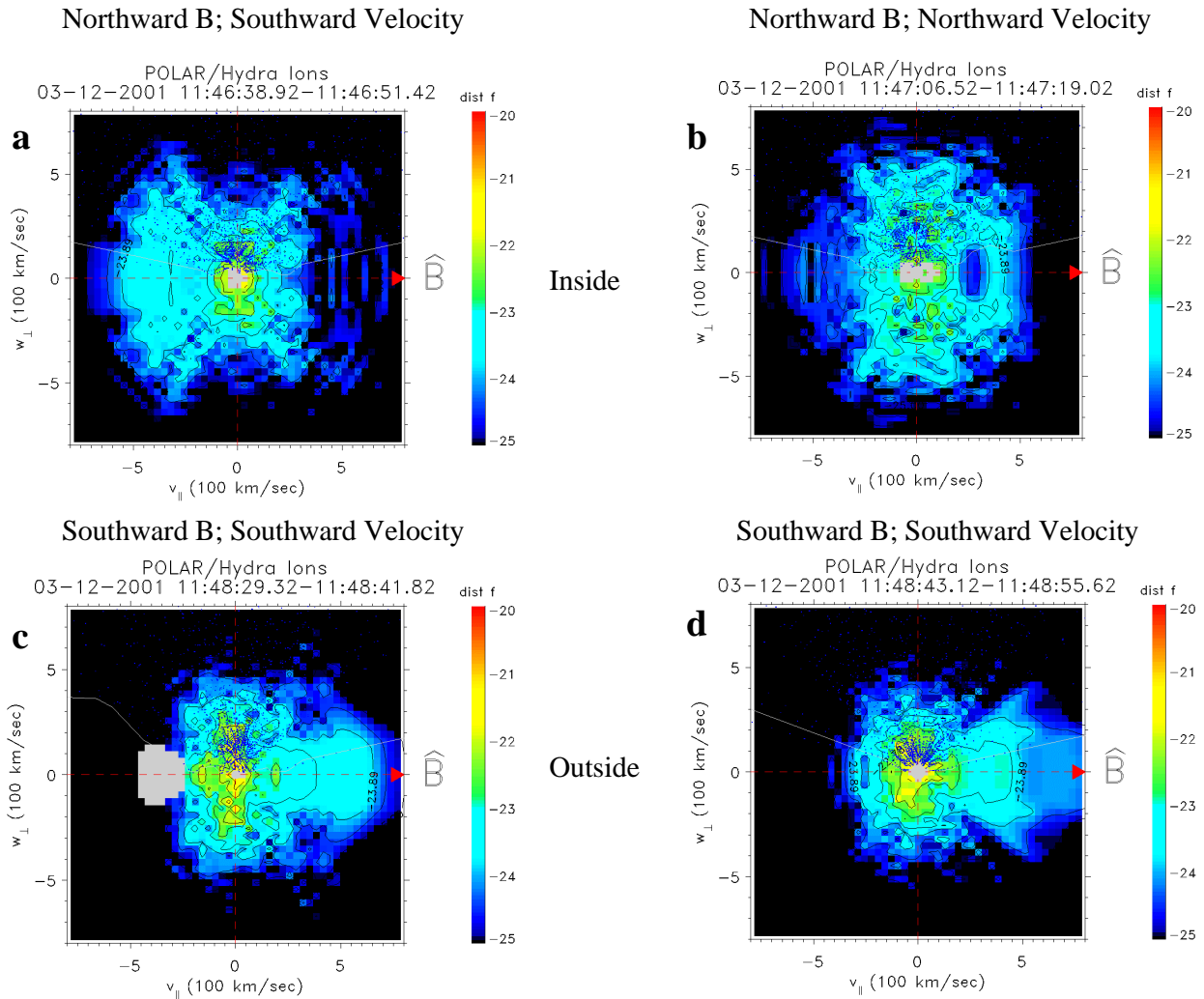
Polar Magnetopause Crossing

Fig. 8. Ion distribution plots for the magnetopause crossing interval indicated by the second circle in Fig. 5.

on the passage through the bow-shock. Coherent passage through the magnetosheath is important for establishing the relative timing and interpretation of Cluster measurements. Note the presence of a magnetic hole centered at ~12:30 UT, when the magnitude of **B** measured at Polar is less than the expected shocked and lagged magnitude from ACE. We note in Fig. 3 that **B** was also smaller at Wind in the middle of this structure, and suggest that ACE did not sample the minimum **B** within the magnetic hole. The clock angle at the time of the magnetopause crossing was approximately 140°, similar to that of the ISM simulation discussed above relative to Fig. 2.

Figures 6b–e depict the energy spectra for the parallel, perpendicular, antiparallel and total ion energy flux. To place these particle measurements in context, Fig. 6a shows Polar measurements of B_Z (red for positive and blue for negative) and B_Y (green trace). The first contact with the magnetopause occurred at 11:39 UT, as indicated by a burst of

antiparallel ions (Fig. 6d). These fluxes occur while B_Y reversed to positive (Fig. 6a) and B_Z (as well as the magnitude of B) dipped. This is a good example of a partial entry into the magnetopause layer. Note too that bursts of parallel and antiparallel ion fluxes were seen during the magnetopause crossing at 11:48 UT. Both of these regions are highlighted by circles and are discussed in more detail below.

Two additional unique features of the spectrograms should be noted. First, there is a lack of plasma in the magnetosheath just outside the magnetopause. In a separate paper, Maynard et al. (2003b) establish that this is a depletion layer. It is one of two types for southward IMF predicted by ISM simulations. Second, magnetosheath particles, including parallel and antiparallel fluxes, are also seen during the passage of the directional discontinuities. These fluxes are intense and have higher energies in the parallel components. Magnetosheath ions are often more biased toward perpendicular "pancake" distributions as the magnetopause is ap-
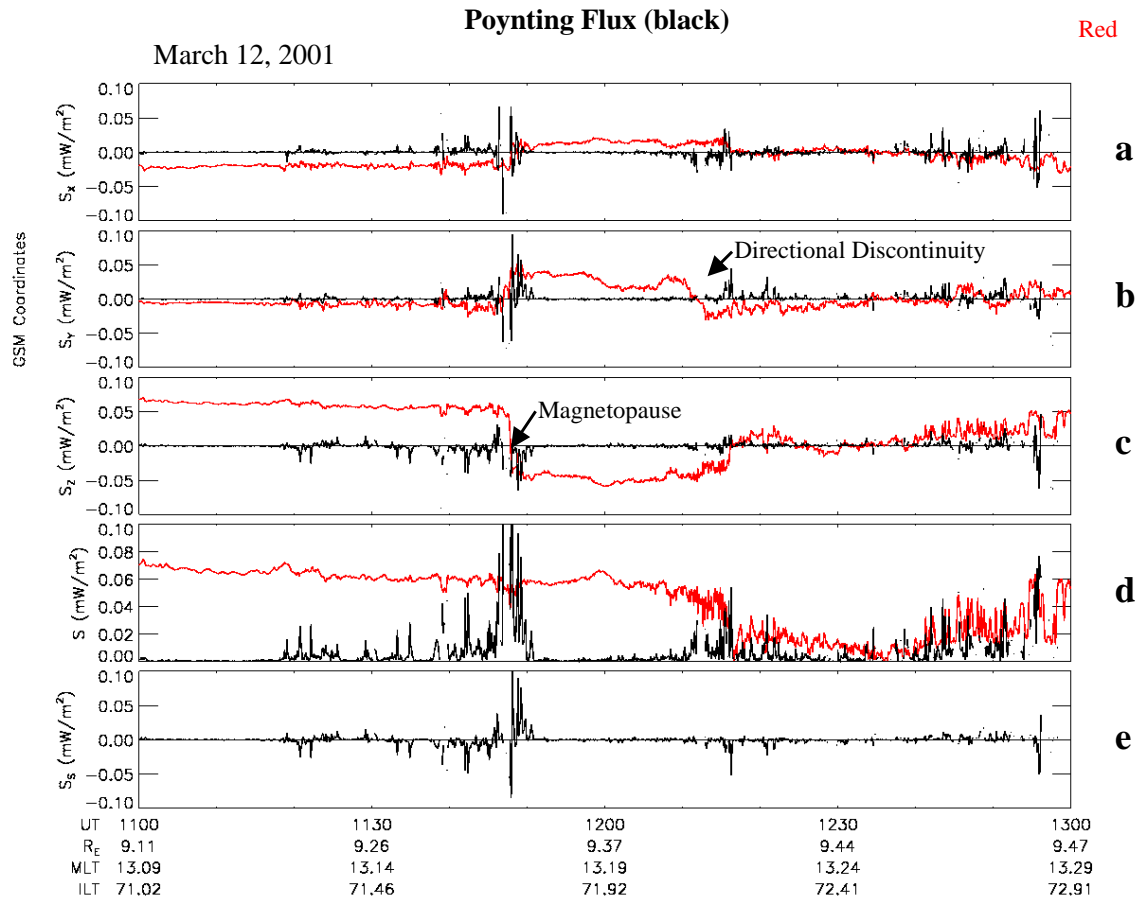
Fig. 9. Wave Poynting flux calculated from $\Delta E \times \Delta B$ and overlaid on the magnetometer traces (red), to provide context, for the 12 March 2001 interval.

proached. The dominance of the perpendicular fluxes is seen in low fluxes of the depletion layer region between 11:50 and 12:00 UT. The various regions are noted at the top of the plot.

Figure 7 shows 3 ion-distribution plots accumulated between 11:39 and 11:44 UT, within the first circle of Fig. 6d. The ion fluxes were shifted in velocity space by the perpendicular electron velocity, as the best proxy for the magnetic field line velocity. To create the distributions, symmetry was assumed around the parallel axis. Points of actual measurement are indicated by black dots (above parallel axis). No measurements exist between the white lines and the parallel axis, as this marks the closest approach of the particle detectors to the magnetic field direction in the analysis interval. For this time when Polar was on the magnetosphere side of the current layer, Fig. 7a shows a cold central core and an accelerated population, well displaced from zero, moving in the negative **B** direction, or coming from north of the spacecraft. From expectations for locations on the inner separatrix (Cowley, 1982), we interpret the accelerated population as being primarily of magnetosheath origin, but with a central core of reflected, accelerated, magnetosphere ions. Figures 7b and c also show similar distributions but with smaller displacements. These distributions indicate a merging-line source to the north of Polar's location.

Figure 8 displays 4 ion-distribution plots at the time of the 11:48 UT magnetopause crossing. Figures 8a and b were taken at locations on the inside of the current layer, while Figs. 8c and d are from locations on the outside of the current layer. Figures 8c and d indicate pancake-like magnetosheath distributions, centered about the origin. An accelerated, cold magnetospheric population is seen along **B**, coming from poleward of the spacecraft. Observed perpendicular energies are comparable to the unaccelerated magnetosphere distributions seen in Fig. 7. Figure 8a depicts an accelerated magnetosheath distribution with the cold magnetospheric background. Again, the acceleration is from north of the spacecraft, which was located at $\sim 16°$ magnetic latitude and 13:10 MLT. In Fig. 8b the distinctions are blurred; however, we suggest that the ion acceleration was weaker and parallel to the magnetic field, or comes from a location equatorward of the spacecraft. How far from the spacecraft is not discernable.

To strengthen our interpretation that these two magnetopause encounters reflect merging events located poleward of the spacecraft, the three components of the wave Poynting vector (**S**) are plotted in Fig. 9. The background magnetic-field components are provided as red lines for reference. Plots in Figs. 9a–d show the three GSM components and the
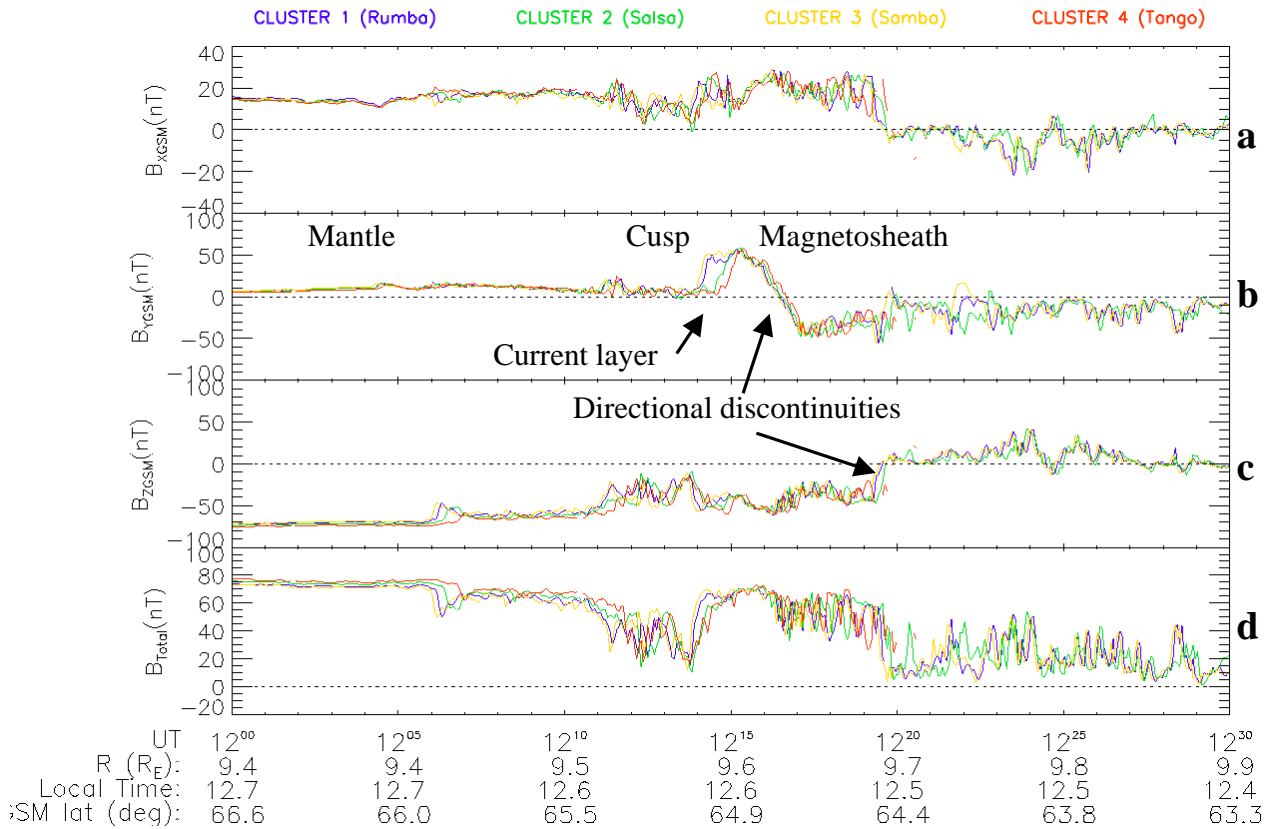
Fig. 10. Cluster magnetic field measurements showing the components and magnitude during the passage of the satellites above the cusp. Color codes for the traces are given at the top. Particular features discussed in the text are highlighted.

magnitude of the wave Poynting flux. Figure 9e shows the component of **S** parallel to **B_0**. Between 11:39 and 11:44 UT S_Z was negative (as was $S_{||}$), in agreement with the direction of the ion acceleration. In the traversal of the magnetopause current layer the calculation was interrupted to avoid contamination. The negative S_Z on the outside of the layer is again in agreement with the direction of particle acceleration. Thus, these two encounters pass our empirical tests for merging events at locations poleward of the spacecraft. In fact, we see enhancements in **S** at 11:39, 11:43, and 11:48 UT, suggesting intensification in the merging rate at those times.

The normal direction for the full magnetopause crossing was found using the minimum variance technique of Sonnerup and Ledley (1974). The normal component was small, but directed outward from the magnetopause, consistent with the merging occurring to the north of the spacecraft. As a further check on the rotational nature of this crossing, a successful Walén test across the full current layer using electrons (Scudder et al., 1999) resulted in a slope of nearly −1, indicating that the source of the rotation is above the spacecraft.

4.4 Cluster observations

Nearer to perigee, Cluster crossed spatial regions more quickly than Polar. Figure 10 presents the three GSM components, and the magnitude of the magnetic field measured by the 4 Cluster spacecraft between 12:00 and 12:30 UT. Cluster exited the mantle into the high-altitude cusp near 12:05 UT and crossed the magnetopause current layer out of the cusp into the magnetosheath between 12:13:50 and 12:15:00 UT. The magnitude of **B** increased as the satellites exited the high-altitude cusp. The biggest change during this crossing event was in the *Y* component. Each of the spacecraft saw the change at slightly different times, with Cluster 3 (Cluster 4) observing the change first (last), indicating that the change is primarily of a spatial nature. The order of crossing (3, 1, 2, 4) is consistent with the spacecraft configuration shown in Fig. 1c, showing Cluster 3 (4) leading (trailing). The subsequent B_Y reversal between 12:16 and 12:17 UT did not result from Cluster crossing back into the cusp. Rather, it reflects the encounters with the first of two IMF directional discontinuities observed earlier by Polar. Note that all four spacecraft

Lag keyed to IMF reversal
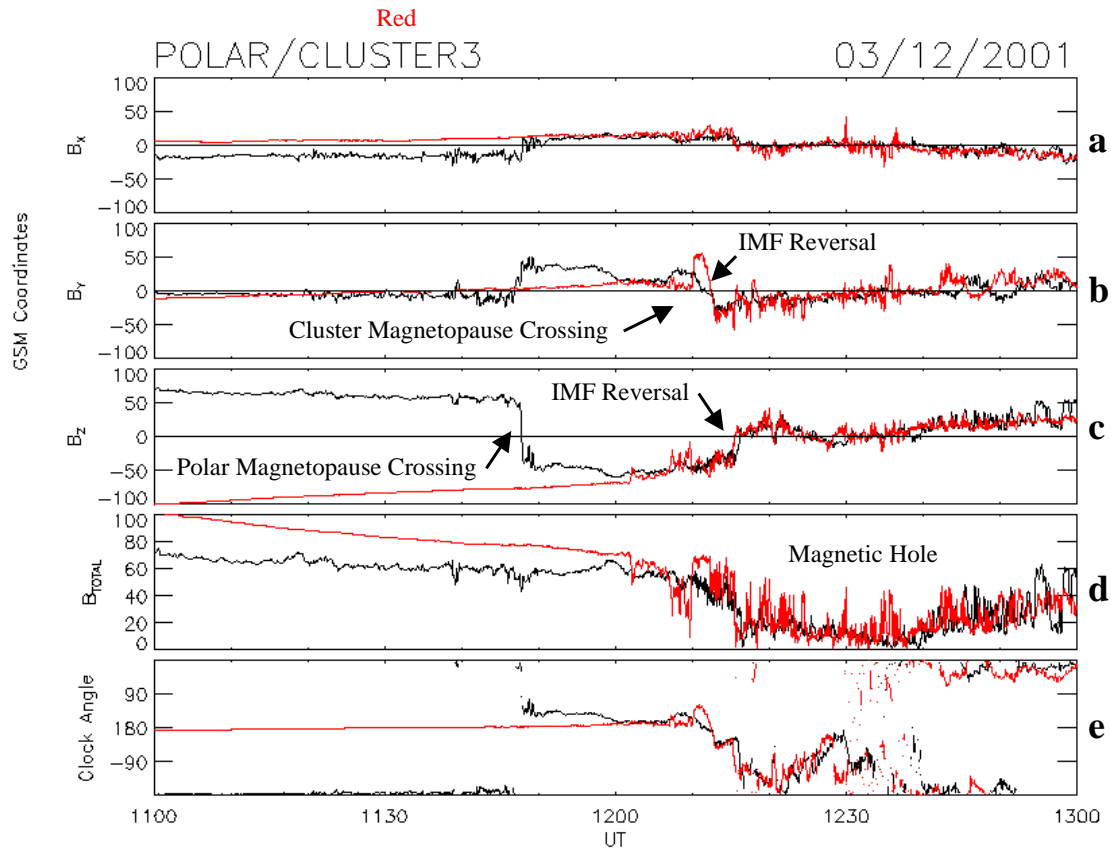
Fig. 11. Overlay of the Polar and Cluster 3 magnetometer data. The Cluster data is delayed −4 min. Note that once Cluster has exited the current layer at the boundary the measured magnetic fields in the magnetosheath match in magnitude, direction and clock angle.

detected the negative shift in B_Y at nearly the same time, indicating that this change is temporal. For a magnetosheath velocity of 100 km/s it would take 6 s for a feature to cross the satellite configuration. In fact, with a 4-min lag Cluster and Polar data are in excellent agreement after 12:15 UT. Figure 11 compares Cluster 3 and Polar magnetic field data with this lag applied to the Cluster measurements. B_Z subsequently also reversed polarity as it did at the location of Polar. At that time the magnitude of B also decreased. Because Polar saw the same directional and magnitude changes in the magnetosheath, we can safely conclude that these exhibit magnetosheath features rather than a reentry into the cusp. Key features of the combined data set are marked by arrows. As the constellation penetrated further into the magnetosheath, the lag between Polar and Cluster observations decreased slightly. This fits expectations, since the observations are made before the structure fully draped over the magnetopause. Minimum variance analysis of the magnetic field from each of the Cluster spacecraft at the magnetopause

crossing and the directional discontinuities provided normals that were stable between the spacecraft. They were also stable between the magnetopause crossing and the B_Y reversal, indicating that the discontinuity was draped along the magnetopause orientation. All of the structure detected between 12:13 and 12:17 UT was planar on the scale of the spacecraft separation and aligned parallel to the magnetopause boundary. The normal to the B_Z reversal near 12:20 UT was similar, but slightly tilted.

Figure 12 presents spectrograms of ion energy fluxes measured in the antiparallel (140°–180°) and perpendicular (80°–1°) direction by CIS on Cluster 3, Cluster 1 and Cluster 4. In all cases the parallel flux (not shown) was much weaker. Three distinct features, which occur at staggered times, are highlighted by dashed lines. The first is an increase in energy seen at 12:06 UT by Cluster 3, 12:06:10 by Cluster 1 and 12:06:50 UT by Cluster 4. The increase is more pronounced in the antiparallel fluxes. The second feature is similar, occurring between 12:10:50 and 12:11:30. The
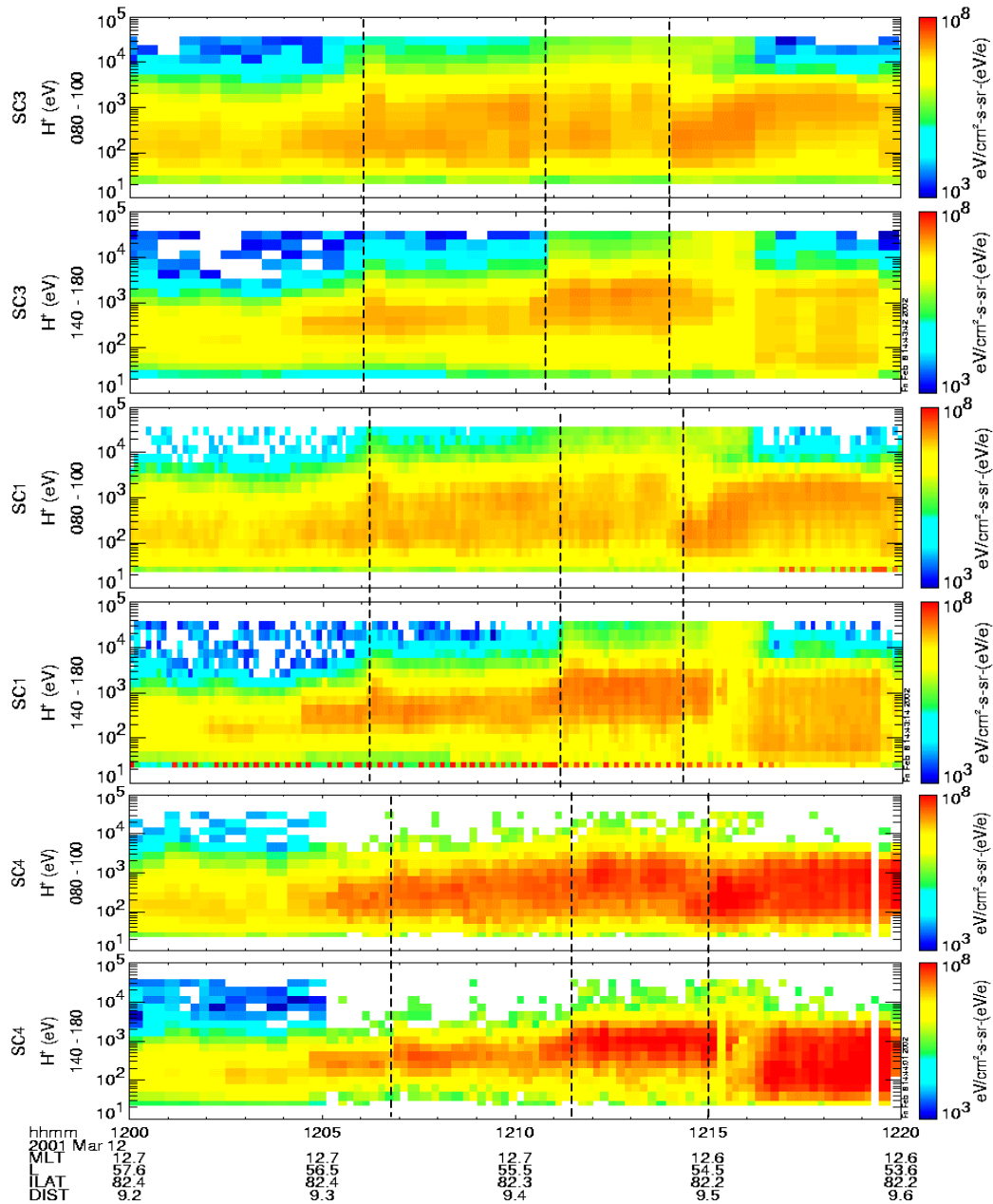
Fig. 12. Ion energy spectrograms measured by the CIS instruments on Clusters 1,3 and 4. Antiparallel and perpendicular fluxes are shown for each spacecraft. Cluster 3 is shown first as it is the lead spacecraft (see Fig. 1c).

third feature was seen in the perpendicular fluxes starting at 12:14 UT at Cluster 3. In this case the intensification starts at low-energies, then spreads to higher energies. From Fig. 10, we see that this increase started as each spacecraft exited the current layer. After this time ion fluxes are more typical of magnetosheath flowing away from the subsolar stagnation region. Subsequently, measured energies were generally lower and the spectral width broader. Based on ion spectral characteristics, and the clear correlations of the magnetometer measurements with those from Polar, the features subsequent to 12:16 UT are of magnetosheath and solar wind origin. Between 12:14 and 12:15 UT the antiparallel fluxes are intense

and higher in energy at Cluster 4, as expected from an active merging site located equatorward of the Cluster spacecraft.

Figures 13b–d show from Cluster 4 perpendicular H^+ velocities (V_H in blue) overlaid onto $E \times B$ velocities (V_E in magenta) in GSM coordinates for the interval between 12:00 and 12:20 UT from Cluster 4. The velocities compare very closely. A 1.5 mV/m sunward electric field offset has been subtracted from the GSE X-axis EFW electric field data to make this comparison. The magnitude of the offset was selected to maximize the correlation. Sunward directed error fields are related to asymmetries in the spacecraft sheath caused by photoemission (Cauffman and Maynard, 1974).
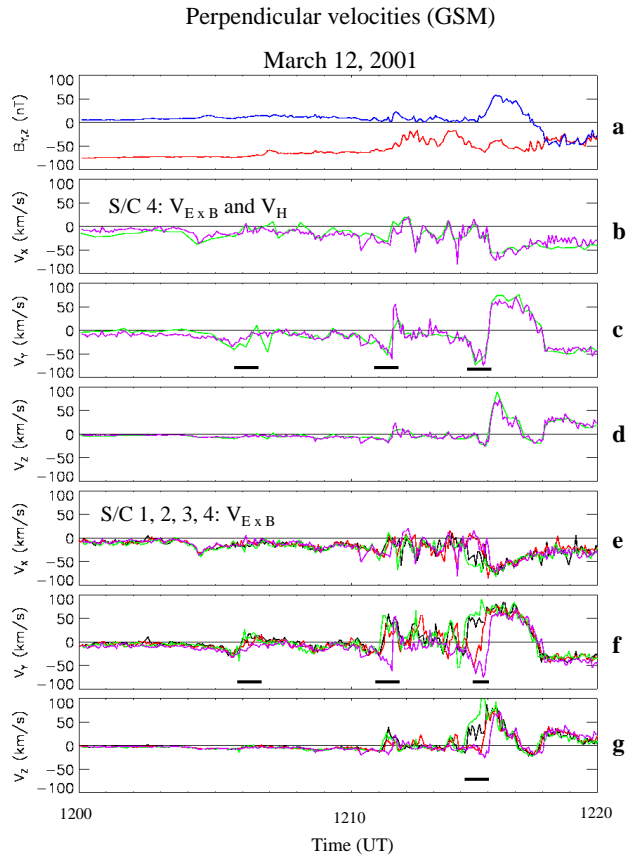
Perpendicular velocities (GSM)

March 12, 2001

Fig. 13. Velocity comparisons from Cluster. **(a)** The Y and Z components of the magnetic field are shown for context. **(b)–(d)** The three perpendicular components of the ion velocity (blue) from Cluster 4 are compared with the velocity determined by $E \times B$. **(e)–(g)** $E \times B$ velocities from all 4 spacecraft are overlaid (1 – black; 2 – red; 3 – green; 4 – magenta).

Figure 13a displays the Z (red) and Y (blue) magnetic field components for context. From Fig. 2 we expect that the velocity in the boundary layer was northward and toward dusk, except where active merging is occurring. Newly-merged field lines are pulled toward dawn soon after the merging takes place. Plasma velocities in the mantle have an anti-sunward component. Three regions of negative excursions in V_{HY} and V_{EY} are seen and are marked by black underscores. Spacecraft 4 was the last of the Cluster spacecraft to traverse the boundary. V_E from all four spacecraft are shown in Figs. 13e–g. Similar offset corrections have been made on each of the other spacecraft. On Cluster 3 a negative excursion in V_{EY} (green) was briefly seen just before 12:14 UT, indicating that this apparent temporal enhancement in merging lasted for over 1 min and had spatial scales on the order of the satellite separation. Other negative excursions in V_{HY} occurred near 12:06 and 12:11 UT, in addition to the larger one between 12:14 and 12:15 UT. Note also the significant positive V_Z, along with the enhanced V_Y that occurs as the spacecraft exit the current layer into the magnetosheath. These velocities are consistent with the pictures in Fig. 2.
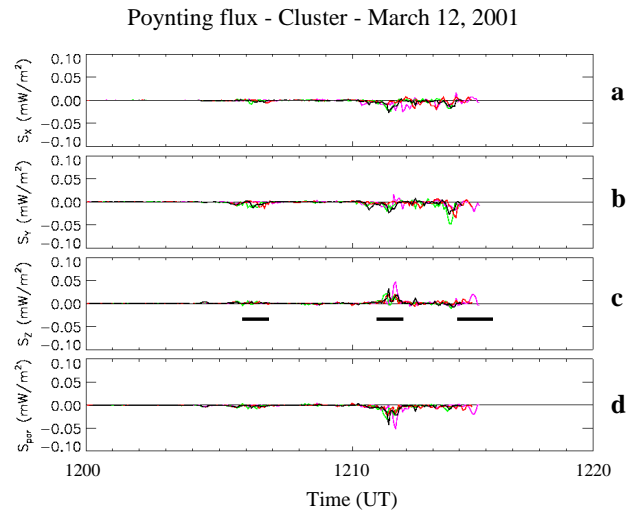
Poynting flux - Cluster - March 12, 2001

Fig. 14. **(a)–(c)** The GSM components of the wave Poynting flux overlaid from all four Cluster spacecraft for the interval between 12:00 and 12:20 UT. **(d)** The parallel Poynting flux overlaid for each of the spacecraft (1 – black; 2 – red; 3 – green; 4 – magenta).

Figures 14a–c present the GSM components of the wave Poynting flux in the same interval from the four Cluster spacecraft, calculated using the same method as with the Polar data. Figure 14d shows the parallel components. The wave Poynting flux is in the antiparallel direction, with peaks in the interval between 12:11 and 12:11:40, indicating that the satellite was above the source. Note the variability between the 4 spacecraft, which indicates that the structure had dimensions of the order of the spacecraft separation. Enhancements are also seen after 12:13:50 UT, but the proximity to the major current layer prevented the determination of the flux through the third region of velocity enhancement in Fig. 13. Small variations were also seen in the first interval of velocity enhancement. All three intervals have been highlighted by the black bar for comparison to Fig. 13. The variability in both time and space suggests that the merging process is non-steady. Considering both the accelerated ions and the Poynting flux, we infer that Cluster is near the outer separatrix of an active merging site equatorward of the spacecraft.

The Cluster configuration was favorable for determining the currents from curl $\mathbf{B}$ (Dunlop et al., 2002). Figure 15 displays local currents derived using a GSM coordinate system centered on Cluster 2. Also plotted are the divergence of $\mathbf{B}$ as a percentage of curl $\mathbf{B}$ and the magnitude of $\mathbf{B}$ at the locations of the four spacecraft. If the calculations were performed without error, Maxwell's equations demand that $\nabla \cdot \mathbf{B} = 0$. Currents determined where the divergence-to-curl ratio exceeds 50% should be treated with caution. In general, for this configuration, the expected error in $\mathbf{J}$ is at minimum 20%. Most of the large values of the divergence occur when the currents are small, highlighting their uncertainty. However, when the currents are large, the divergence ratio is, in general, small, indicating where the calculated currents are
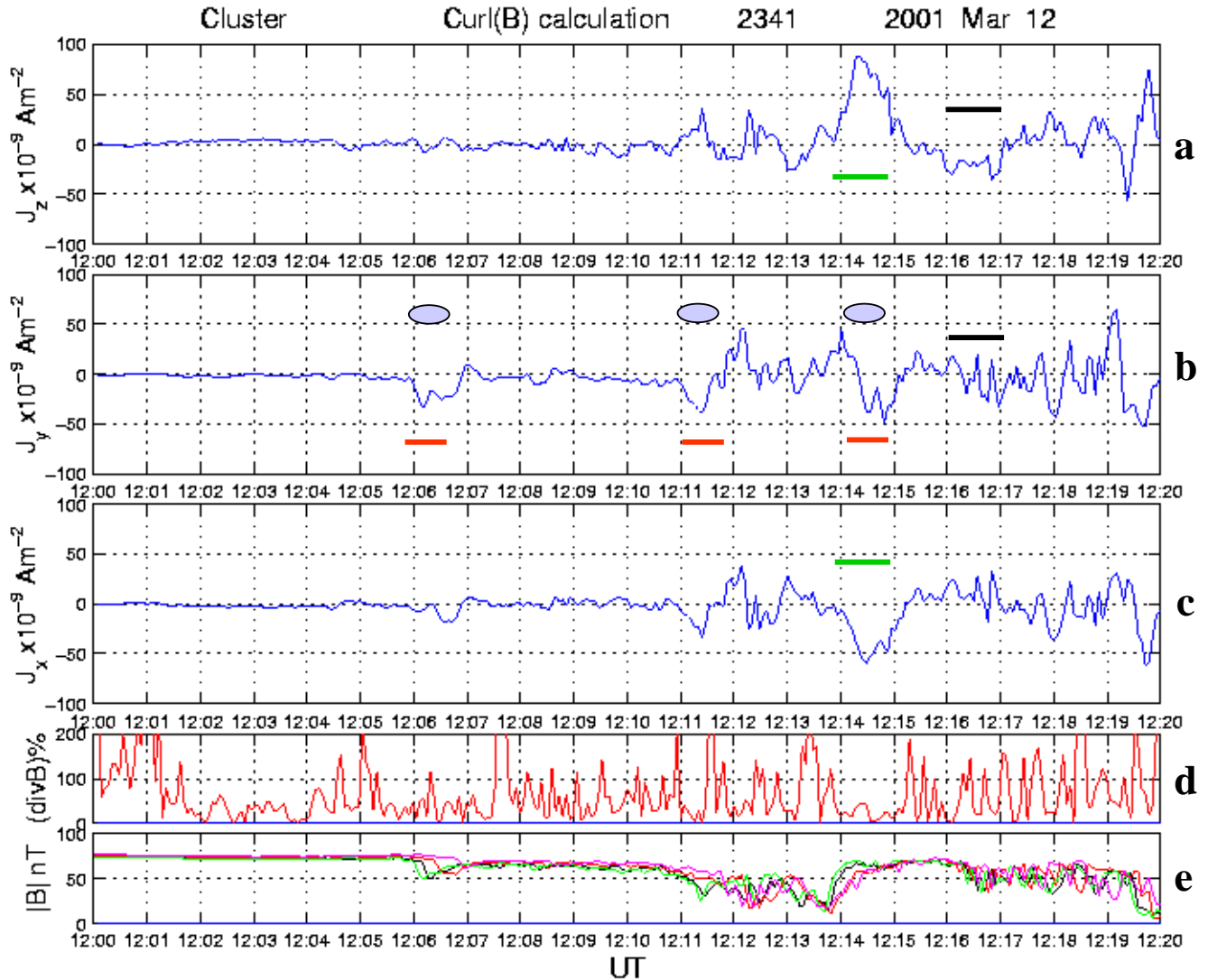
Fig. 15. (a)–(c) Currents in GSM coordinates determined by the Curl **B** calculation. The calculation is centered on Cluster 2. **(d)** The ratio of the divergence of **B** to the curl of **B** expressed in per cent. The ratio provides an indication of where the calculation is reliable (see text). The magnitude of **B** is given in the bottom panel for context.

reasonably valid. The curl **B** calculation integrates the currents over the scale size of the tetrahedron ($\sim$ 600 km). The largest current was detected between 12:14 and 12:15 UT and is primarily in the $+Z$ and $-X$ directions, noted by the green bars. It takes the four spacecraft over a minute to cross the main current layer, indicating its temporal stability. Thus, the center of this current should be well resolved. Counterclockwise Chapman-Ferraro currents on the dusk edge of the cusp have the anticipated direction. Note that between 12:16 and 12:17 UT, when the directional discontinuity was crossed, the current determination was less accurate; however, the direction was $-Z$, opposite to the Chapman-Ferraro currents, confirming our interpretation that Cluster did not pass back through the boundary current layer.

J_Y is the most variable component showing both polarities, although the strongest are currents in the $-Y$ direction.

Some of the variability could occur if the current scale size was less than that of the Cluster configuration. Currents from structures of scale size less than 600 km may suffer from this error. Attention is directed to negative J_Y excursions observed between 12:06 and 12:07, 12:11 and 12:11:40, and 12:14:30 and 12:15 UT, marked by red bars. There is also an associated smaller $-J_X$ excursion. These correspond to times when negative V_{HY} and V_{EY} excursions were observed by the Cluster spacecraft (black bars in Fig. 13). This suggests that these currents are related to temporally varying merging. Close to these times enhanced parallel ion and Poynting fluxes, our indicators of merging, were detected. The merging site must be south of the spacecraft, and the merging rate must be varying on minute scales to produce the observed three pulses. When we consider that Polar was showing temporally varying merging at high latitudes 20 min

previous, the implications are that this also involves time-varying high-latitude merging. The next section relates these enhancements to intensification of ionospheric plasma velocities measured by SuperDARN radars.

4.5 SuperDARN measurements

Each SuperDARN radar measures the velocity component toward and away from the transmitter. To infer the large-scale flow pattern, the Ruohoniemi and Baker (1998) "map potential" technique was employed. Line-of-sight (l-o-s) velocity measurements from multiple radars are fitted to an expansion of the electrostatic potential in spherical harmonics, to yield large-scale global convection maps. First, the l-o-s data are filtered and mapped to a polar grid. These "gridded" measurements are then used to determine a solution for the electrostatic potential distribution that is most consistent with the available measurements. Velocities should fall along plasma streamlines in the modeled pattern. Backscatter targets within the radar field-of-view are not always available, and significant areas exist outside the reach of the radar system. The statistical model of Ruohoniemi and Greenwald (1996), parameterized by IMF conditions, is used to stabilize the solution in regions where no measurements are made. Figure 16 presents dayside Northern Hemisphere ionospheric convection patterns, each averaged over the interval given at the top. Dotted concentric semicircles indicate lines of constant magnetic latitude in 5° increments. Noon is located at the top of each pattern. During the period from 11:00 to 12:15 UT, SuperDARN was observing velocity enhancements in the 14 to 15 MLT region between 70 to 75°. Figures 16a and b show these enhancements by comparing two consecutive patterns near the 11:48 UT Polar magnetopause crossing. The orange circle highlights the region of velocity enhancement, indicated by increased numbers of red drift vectors in the right pattern compared to the left. Note that the enhancement is localized, in the same region that the open-closed field line pair is mapped to in the simulation depicted in Fig. 2b, and occurs 1–2 min after the enhanced parallel fluxes were seen at Polar. We suggest that the delay is related to differences in Alfvén travel times. The signature in the ionosphere should lag that in the outer cusp by the order of a minute, due to Alfvén wave propagation time. The SuperDARN patterns show numerous increases in velocity in this general area over the hour-plus period.

To show the time variability, a search was made in the SuperDARN data for the largest velocity in the region and its location. The magnitude, the components, and the location are plotted in Fig. 17. The time of the three enhancements in merging observed at Polar are noted by the vertical red lines. The corresponding velocity peaks at SuperDARN are highlighted by the red dots. Within the interval that Polar was probing the magnetopause, these are the only peaks. Subsequent peaks starting at 12:06 UT correspond to the interval where Cluster observed evidence of merging. Figures 16c and d show SuperDARN potential patterns and vectors for intervals that contain the first 2 velocity and cur-

rent enhancements at Cluster, depicted in velocities in Fig. 13 and currents in Fig. 15. Returning to Fig. 17, the velocity and current enhancements observed by Cluster and noted by the blue dots correspond to three velocity enhancements seen at SuperDARN. Those periods are noted by the blue ovals in Fig. 15. Since Cluster observations come from above the cusp on the outer separatrix, while SuperDARN is looking at the response at the foot of the field line, we suggest that the difference in times from Alfvén wave propagation may be less than those observed by Polar. Note that no peaks above $800 \, \mathrm{m \, s^{-1}}$ occur after 12:15 UT. The velocity enhancements are in the region predicted by the simulation as being tied to high-latitude merging. The correspondence with the Polar magnetopause merging encounters suggests that SuperDARN and Polar are observing the opposite exhaust regions of a time-varying active high-latitude merging line. Continuing the correlation with Cluster, we are able to relate 3 more peaks in the SuperDARN velocities to time varying merging. The implications from considering the 2-h period of SuperDARN velocities is that the rate of merging varies often and considerably. The location may be just as variable.

4.6 Summary of the 12 March observations

From the observations presented above we may conclude for this day when the IMF clock angle was about 140° that:

1. Polar, while skimming the nose of the magnetosphere, observed the effects of merging at high latitudes. Accelerated ions and wave Poynting flux were used as discriminators for the existence of merging. While the exact location of merging is not discernable from the data, it was above the spacecraft, which, in turn, was well above the component merging line location of Gonzalez and Mozer (1974).

2. The merging rate was temporally varying, as indicated by both Polar and Cluster measurements.

3. SuperDARN observed enhancements in the flow in the ionosphere associated with these time-dependent merging events observed at Polar. Polar, near the subsolar magnetopause and SuperDARN in the high-latitude ionosphere, monitored both exhaust regions. From SuperDARN observations we may also infer that variations in the merging rate occurred continuously for more than an hour.

4. Cluster continued the correlation, placing the merging location below the satellite, which was located above the cusp. Both SuperDARN and Cluster observed effects of time-varying merging.

5. Flow in the boundary layer and adjacent magnetosheath was generally away from the sub-solar region unless specifically diverted by merging. In a time dependent process, boundary layer flows vary continuously.

6. Two directional discontinuities and an associated magnetic hole were imposed on the magnetosphere system

SuperDARN - March 12, 2001

1148-1150 UT

a

1150-1152 UT

b

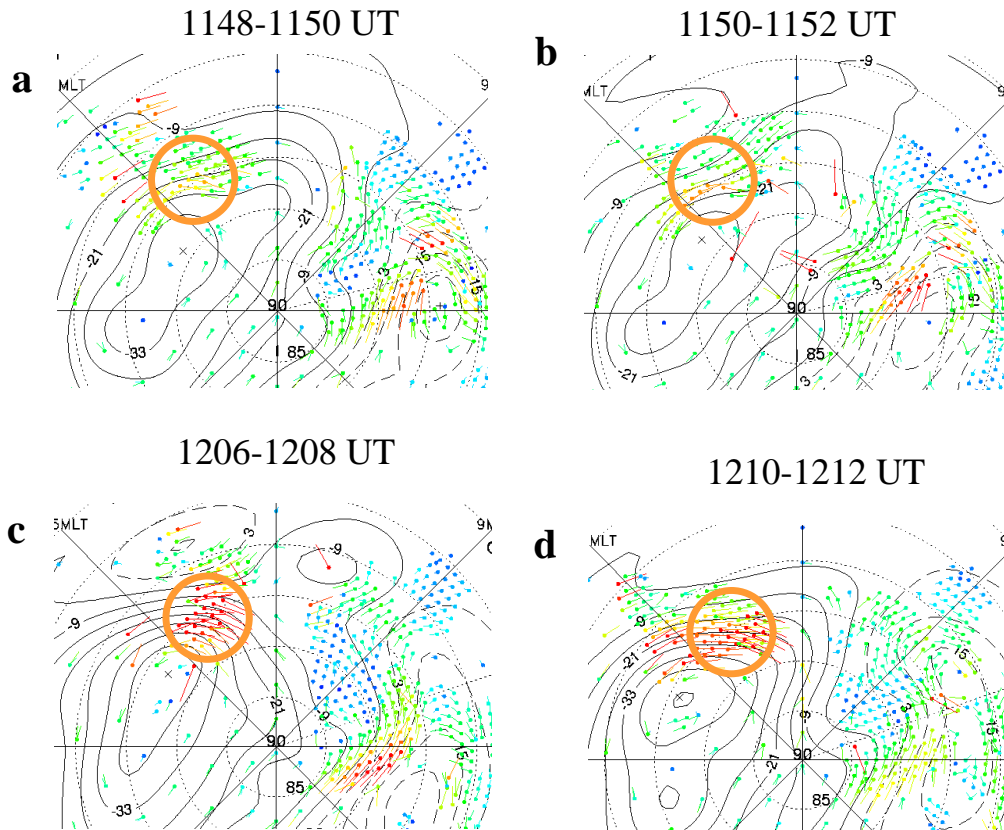### 1206-1208 UT

c

1210-1212 UT

d

Fig. 16. Potential patterns and drift vectors determined from SuperDARN measurements for 4 intervals related to merging observations at Polar and Cluster. The regions of interest are highlighted by the orange circles.

from the solar wind. The effects of these were observed by both Polar and Cluster.

7. Adjacent to the magnetopause, Polar observed a depletion layer, implications of which are further discussed by Maynard et al. (2003b).

5 Other events

Table 1 summarizes all of the merging events investigated to date, using wave Poynting flux and accelerated ions as discriminators. The events are organized according to the applicable IMF clock angle (third column). The fourth column lists our best estimates of the merging locations. Note that the measurements provide information about whether the site is to the north or south the spacecraft. For a number of events we calculated the difference between the spacecraft location and the component merging line of Gonzalez and Mozer (1974). The differences are listed in the last column. During periods when the ions and Poynting flux propagated from north of Polar and the differences are significant, we labeled the merging location as being at high latitudes. The last column also comments on special circumstances prevail-

ing during each pass. If the ions and Poynting flux originated south of Polar, we were unable to discern from the measurements alone, whether the merging line is near the equator or at high southern latitudes. Question marks indicate instances when assigned merging locations are ambiguous. The event of 05:48 UT on 1 April 2001 is labeled "close" because Mozer et al. (2002) interpreted signatures obtained during this magnetopause crossing as indicating proximity to the separator. In some cases we relied on SuperDARN measurements and ISM predictions to identify merging locations. These are noted in column 5. The event at 05:05 UT on 16 April 2000 included episodic encounters with fluxes from the north and south of the spacecraft. We address this further in the discussion. During the two passes of 31 March 2001, Polar did not enter the dayside magnetosphere because of the high activity and very compressed conditions. In each case Polar crossed from the mantle to the magnetosheath above the cusp as noted in the comments.

For applicable clock angles of 150° or less in the events of Table 1, merging generally occurred poleward of the spacecraft and was inferred to be at high latitudes. This conclusion should be substantiated in the analysis of more events; however, it is clear that one must consider high-latitude merg-
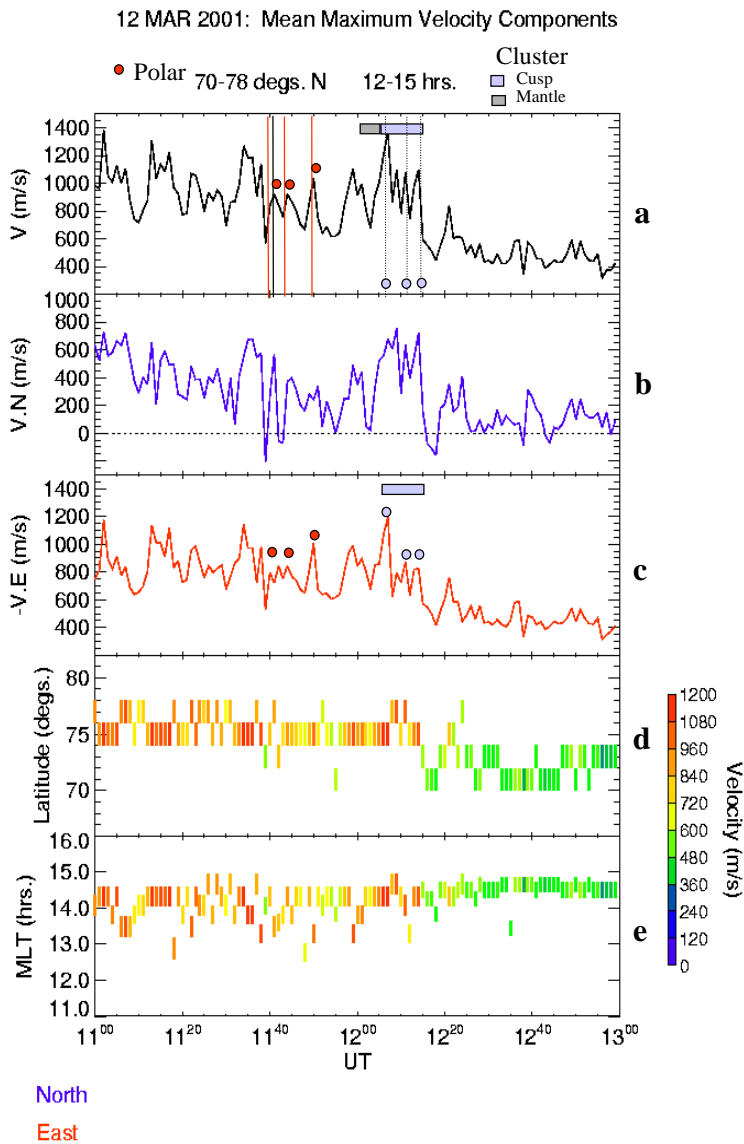
Fig. 17. The maximum velocities and their locations determined by Super-DARN for the interval between 11:00 and 13:00 UT.

ing as an option when interpreting events driven by a significant IMF B_Y. Our measurements suggest that low-latitude or component merging is indicated only when B_Z was the dominant IMF component.

6 Discussion

We have used observations of accelerated particles and wave Poynting vectors as our primary indicators as to whether merging has occurred and, if so, where. As demonstrated above, both flux types provide necessary, but not sufficient, conditions for identifying merging events. Establishing that the boundary is a rotational discontinuity adds a third necessary indicator of merging. Since rotational discontinuities may be found in any magnetohydrodynamic flow, including those that do not involve reconnection, a successful Walén test, by itself, is not a sufficient test to conclude

that merging geometries have been encountered. However, the magnetopause-sheath interface is generally thought to include such a structure to form a locally open boundary. In this spirit a successful Walén test (with electrons) with slope ±1 is associated with a potential merging site, whose X-line separator will, in general, be well removed from the spacecraft's trajectory. Successful Walén tests to establish the rotational discontinuities, in conjunction with observations of accelerated particles, have been the primary empirical criteria for identifying merging events. Recently, Scudder et al. (2002a) reported small-scale breaking of both ion and electron gyrotropy, as well as parallel electric fields within merging regions poleward of the cusp during an interval of northward IMF. In the events considered here, observations were made away from the separator region. Thus, we rely on signatures recognized as strong indicators, but not conclusive proof, that merging has occurred. With this caveat in

Table 1. On the location of merging with varying clock angles

Date	Time	Clock angle	Merging Location	Discriminators	MLT	MLAT	Height: Comments
04/16/00	07:03–07:10	~90	SH (high-latitude)	Ions, SuperDARN, ISM	11.4	22.7°	30°
04/01/01	05:20–05:22	~130	NH(high-latitude)	Ions	11.7	3.4°	11.2°
04/01/01	05:33–05:36	~130	NH(high-latitude)	Ions, S?	11.7	4.6°	12.3°
04/01/01	05:57–06:00	~135	NH(high-latitude)	Ions, S	11.8	6.8°	13.8°
03/12/01	11:39–11:44	~140	NH (high-latitude)	Ions, S, SuperDARN	13.2	15.5°	10.5°
03/12/01	11:48:11:50	~140	NH (high-latitude)	Ions, S, Walén, SuperDARN	13.2	16.5°	11.0°: Separator depletion layer post-noon – By positive Cluster. Depletion layer at Polar indicates high-latitude
03/12/01	12:06–12:15	~150–160	NH (high-latitude)	Ions, S, SuperDARN			
03/31/01	06:08–06:20	~160	Above spacecraft (above equator in NH?)	Ions, S, ISM	11.3	−30.5°	Polar crosses MP below SH cusp, sees outer separatrix, Shoulder depletion layer
04/01/01	05:46–05:48	~160	Above spacecraft (close?)	Ions	11.8	5.7°	12.1°
04/01/01	05:28–05:32	~160	Below spacecraft (equator?)	Ions, S	11.7	4.2°	10.7°
04/16/00	04:50–04:55	~180	Below spacecraft (equator?)	Ions	11.1	7.1°	7°
04/16/00	05:05–05:20	~180	Below and above SC (equator and higher latitude)	Ions, S?, $E \times B$	11.2	9.5°	9°: Moves off equator from dipole tilt and increase in B_x
04/16/00	07:30–07:40	~180	Below spacecraft (equator?)	Ions, S, SuperDARN	11.5	26.0°	24°: Separator depletion layer pre-noon after 08:00 UT – By negative
03/31/01	16:00–16:20	Near 180	Below spacecraft (below equator in SH?)	Ions, S, ISM	12.1	48.1°	Polar crosses MP above NH cusp, sees outer separatrix, Shoulder depletion layer

mind, we proceed by assuming that Polar detected signatures of actual merging events. We first comment on the use of Poynting flux as a discriminator. We next comment on some spatialtemporal implications of the observations.

6.1 Wave Poynting flux as a merging discriminator

When electron gyrotropy is broken and merging takes place at an X-line (Scudder et al., 2002a), magnetic field energy is converted into particle kinetic energy, and the magnetic field configuration in the "diffusion" region changes. This information must be conveyed away from the separator along the merged field lines. Atkinson (1992), following earlier calculations by Sonnerup and Wang (1987), showed that Alfvén waves propagate away from the diffusion region, carrying the field-aligned currents (FAC) needed to discharge Hall electric fields that develop in the collisionless merging process. These FACs are carried by electrons (since the ions cannot respond in these thin layers) with relatively large drift speeds parallel to **B**, having parallel electron Alfvén Mach numbers as high as 4, as recently been reported by Scudder et al. (2002a). These parallel currents can be seen to flow along the separatrices in the Hall MHD simulations of Ma and Bhattacharjee (2001). FACs are carried by obliquely propagating Alfvén waves (Siscoe, 1983). We expect to detect Alfvén waves propagating away from active merging sites along the separatrices.

Wave Poynting vectors were calculated using CRRES electric and magnetic field data by Maynard et al. (1996a), to determine locations of energy release at substorm onset. While most calculations were performed with spin-averaged

measurements, Maynard et al. (1996b) were able to achieve higher time resolution using despun data acquired during one CRRES pass. No significant power was found at frequencies above the Pi-2 range, covered by spin-averaged electromagnetic fields. A similar test was performed here. The power levels in both the high resolution E and B were significantly less at higher frequencies than at frequencies below the ion gyrofrequency. A check of the angle between **S** and **B** indicated that **S** was nearly field-aligned during the enhancements at the magnetopause. Thus, the data are consistent with Alfvén waves occurring at the magnetopause encounters where merging is claimed. The magnitudes of wave Poynting vectors generally peak below one-third to one-half of the total Poynting flux values. The peaks occurred at places where Polar encountered accelerated ions.

A further example of wave Poynting flux observations at a merging separatrix, from 31 March 2001, is given in Fig. 18. In this pass Polar crossed from the Southern Hemisphere mantle directly into the magnetosheath, without encountering the dayside magnetosphere. Figure 18a displays the parallel wave Poynting flux. The magnitude and Y and Z components of **B** are shown in Figs. 18b and c. Figures 18d–f show the parallel, perpendicular and anti-parallel ions. Note that strong fluxes of accelerated parallel ions occurred in coincidence with the parallel wave Poynting flux. Three examples of ion distribution plots are given in Figs. 18g–i. Strong acceleration appears in each spectrum. After encountering these fluxes, Polar entered the magnetosheath, characterized by weak, perpendicular fluxes, identified as a depletion layer (Maynard et al., 2003b). The accelerated particles are in-
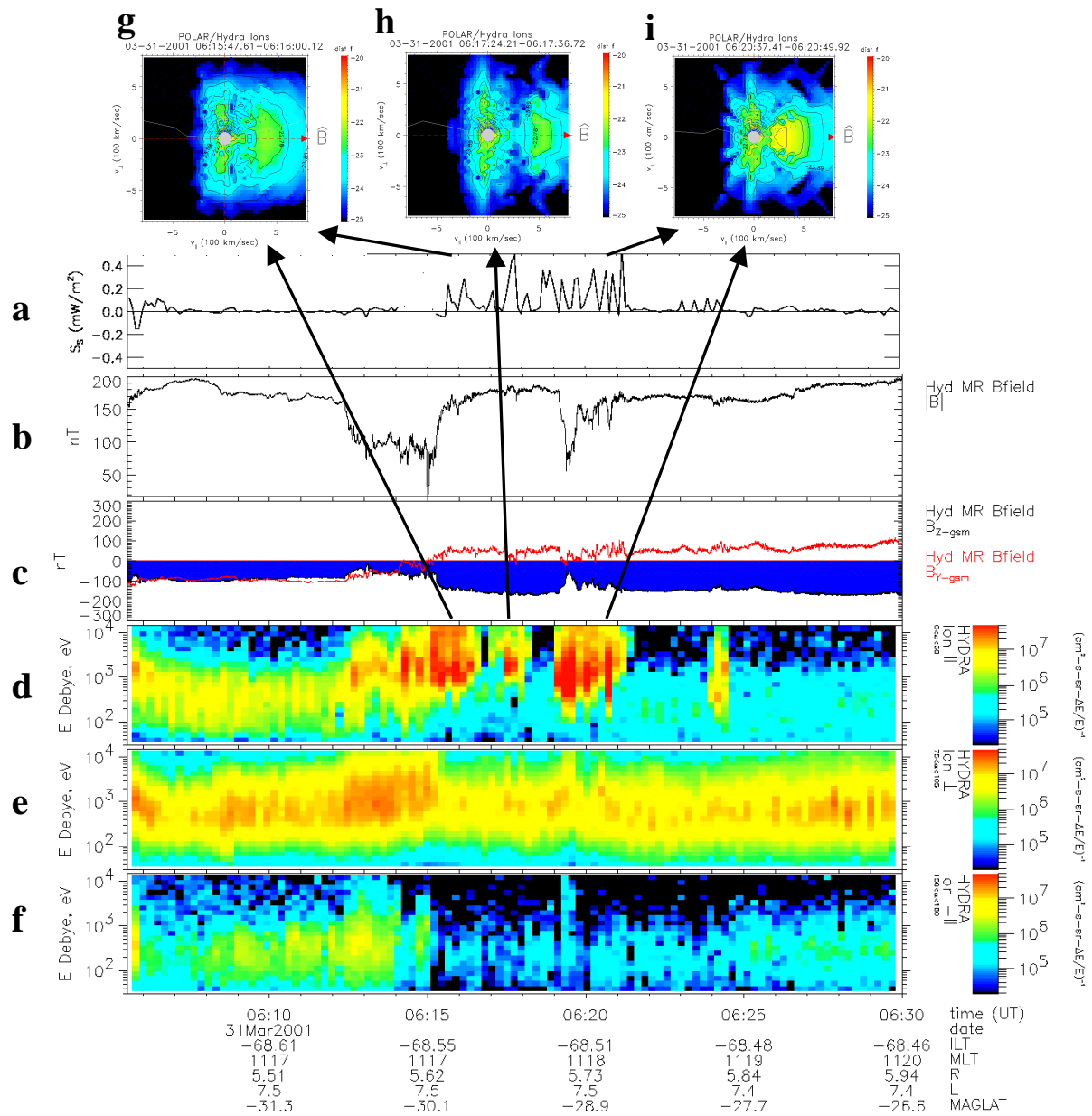
Fig. 18. Correlation of the wave Poynting flux measured by Polar above the cusp on 31 March 2001, with accelerated particles associated with the outer separatrix separating open magnetic field lines from IMF magnetic field lines in the magnetosheath.

terpreted as moving along the outer separatrix from a low-latitude merging site, that divides newly-opened field lines being added to the mantle, from magnetosheath field lines tied to the IMF on both ends.

We conclude that the wave Poynting flux provides a good discriminator to indicate when merging takes place and the direction of the merging site with respect to the measuring spacecraft. However, sources of Alfvén waves other than merging may be available. Thus, their presence must be classified as necessary but not sufficient as a condition to establish that merging is occurring.

6.2 Location

The 12 March data indicate that Polar detected signatures of merging events, far removed from a near equatorial component merging line (Gonzalez and Mozer, 1974). This is true for many events listed in Table 1 with IMF clock angles $< 150°$. The measurements indicate that merging occurs at high latitudes under a variety of conditions. In other events the particle and Poynting fluxes were clearly propagating from south of the spacecraft. These signatures appear to be consistent with either component merging near the equator or antiparallel merging at high latitudes in the conjugate hemisphere.
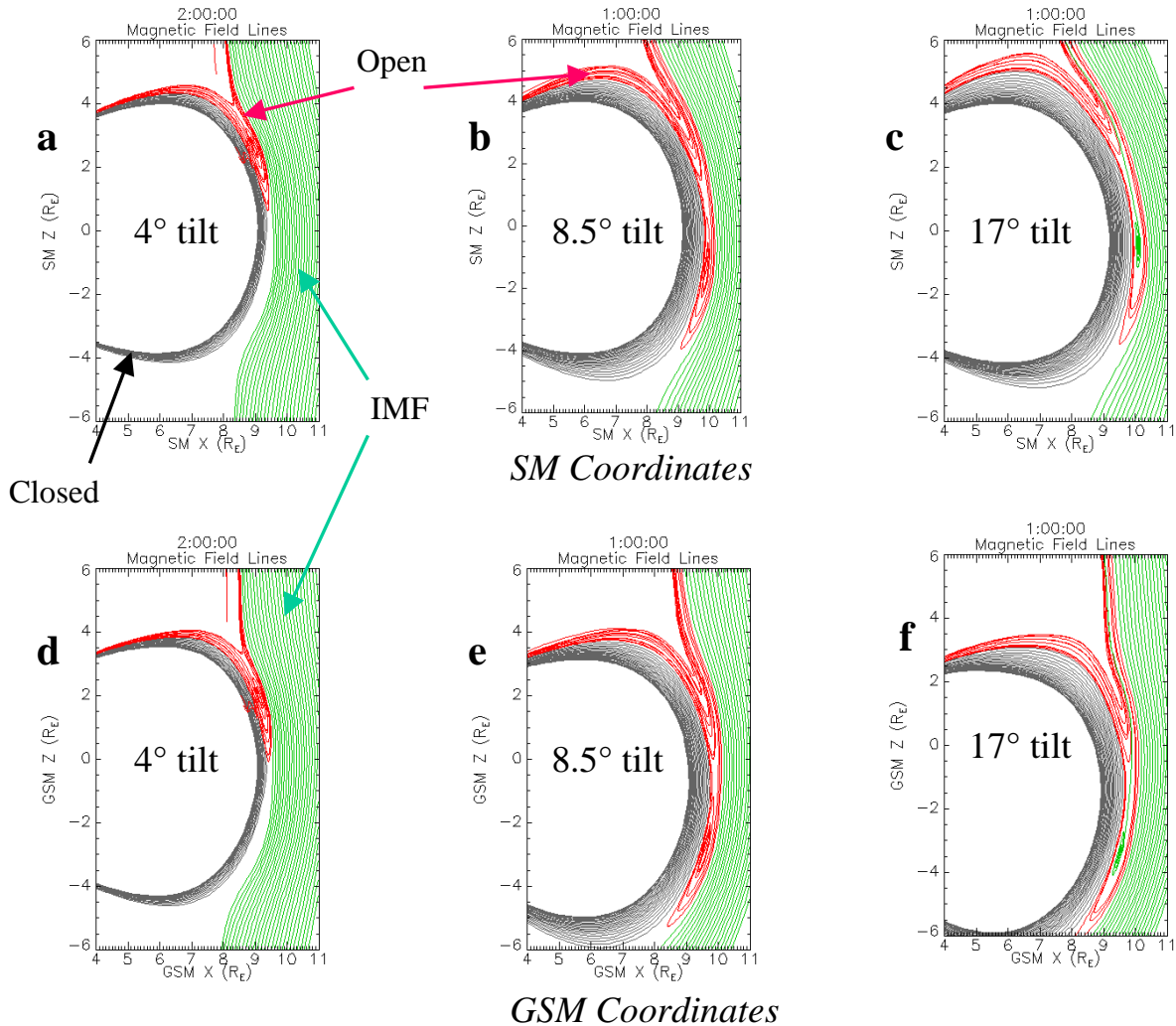
Effect of dipole tilt on merging site for IMF southward

Fig. 19. Traced magnetic field lines using MHD simulations with three different dipole tilt angles using ISM. Black field lines are closed. Red field lines are open with one foot in the Northern Hemisphere. Green field lines have both feet in the solar wind. The results are presented in both SM and GSM coordinates.

An intriguing event occurred on 16 April 2000, when the IMF clock angle was near 180°, but the inferred merging site was to the north of the Polar's location. The measurements were made at ∼05:20 UT, when Earth's dipole axis tilted toward midnight. We have conducted a series of ISM simulations with increasing dipole tilts to determine whether off-equatorial merging can occur with 180° clock angles. Figure 19 displays traces of magnetic field lines that are closed (black), have one foot in the Northern Hemisphere (red) or have both feet in the interplanetary medium (green), for 3 different dipole tilt angles. Simulation results are presented in both *SM* and GSM coordinates. In both coordinate systems the red (open) field lines indicate that for dipole tilts ≥ 8°, merging moves away from the equator to higher latitudes. These are not extreme tilt angles. These conditions are met every day as the dipole rotates with UT. We note

that ISM simulations incorporate current-dependent explicit resistivity, which typically turns on near the equatorial magnetopause to force dissipation, to aid merging. The code can place dissipation wherever it chooses via PDM to keep gradients in check. Thus, ISM predictions of merging away from the equator indicate a clear preference of the code for high-latitude merging. Recall too that B_X serves to increase or decrease the effective dipole tilt (e.g. Crooker, 1992). Thus, over the course of the day at particular UTs merging may be preferred away from the equator, even with a nearly southward IMF. Thus, one should not automatically assume that merging must be confined to low latitudes. We have added question marks in Table 1 to events with particle and field signatures indicating merging sites south of the spacecraft. In some cases, when B_Y is significant, we suggest that merging locations may be southern high latitudes.

Two events on 31 March 2001 are called "shoulder" events in Table 1, one of which is discussed above relative to Fig. 18. The observations were made near the outer separatrix, poleward of the cusp. Shoulders occur under strongly driven conditions, when the magnetic field poleward of the cusp is increased by currents flowing in the Region 1 solenoid. (Siscoe et al., 2002). These currents close across the polar cap and over the high-latitude magnetosphere. The fringing field of this solenoid depresses the magnetic field in the subsolar region, creating effective magnetic shoulders above the cusp. Other implications of these shoulders are presented in Maynard et al. (2003b). Certain dipole tilt angles accentuate these shoulders and, based on the results displayed in Fig. 19, could move the merging site away from the equator.

The ISM and observational results suggest that merging at high latitudes is a common occurrence. Figure 2 illustrates high-latitude merging in simulations with a clock angle of 135°. Component merging exists in that same simulation near the equatorial magnetopause. It was aided by explicitly included equatorial resistivity in the simulation. Over the past two decades, component merging was assumed by many to be the rule, rather than the exception. A recent study by Moore et al. (2002) concluded that merging rates should be appreciable near the subsolar magnetopause for most IMF clock angles. To explain DMSP particle characteristics in the cusp, Wing and Newell (2001) argued that both subsolar and high-latitude sources simultaneously coexist. Two high-latitude sources may also work. The results of Maynard et al. (2001b) require high-latitude sources in both hemispheres to reconcile the timing differences. Further work is needed to establish how the location of merging varies with IMF input.

6.3 Temporal characteristics

To date, the 12 March event is unique in that measurements from three separate locations were integrated to address the temporal aspects of the merging event. Whenever the merging rate increases, we expect that the magnetopause erodes inward slightly. This apparently was true at 11:39 and 11:48 UT, when Polar observed the effects of merging at northern high latitudes. The temporal nature of the process is further confirmed by the SuperDARN observations. Using Fig. 2 to understand the global context, we are able to correlate the velocity enhancements observed by SuperDARN near 13:00–15:00 MLT with the changes observed by Polar. These correlations continued in observations above the cusp by Cluster. We infer that SuperDARN observations primarily reflect temporal dependence of merging. Between 11:00 and 12:15 UT, multiple peaks in ion velocities observed by SuperDARN suggest that the merging rate and/or location varies on time scales of 2 min, to 8–10 min, commonly associated with flux-transfer and pulsed-reconnection events (e.g. Cowley and Lockwood, 1992). Maynard et al. (2001b) reported observations of temporal effects of merging processes on time scales of 1 to 3 minute. The remote observations of 12 March show effects in both exhaust regions, with merging varying on similar short temporal scales.

7 Summary and conclusions

The location and temporal dependencies of dayside merging have been investigated from a global perspective. Measurements made in diverse regions of near-Earth space constrain interpretations through demands for consistency between observed phenomena. Data acquired on 12 March 2001 near the subsolar magnetopause, in the high-altitude cusp, and in the ionosphere, indicate that merging occurred at high latitudes in a time-varying manner. We have used simultaneous detection of field-aligned wave Poynting flux and accelerated ions as the primary, remote discriminators of merging. For a period of time with the IMF clock angle at $\sim 140°$ merging developed to the north of Polar, well removed from predicted locations of component-merging lines (Gonzalez and Mozer, 1974).

For more than an hour SuperDARN observed enhancements in ionospheric plasma flows near 14:00 MLT, associated with the time-dependent merging observed by Polar. A comparison of observations with MHD simulations of ISM confirms the existence of a high-latitude merging site and suggests that SuperDARN and Polar observed effects attributable to both exhaust regions of a temporally varying X-line. This interpretation is further confirmed with enhancements observed by the Cluster satellites.

From these and other observed results during listed magnetopause encounters, we conclude that merging occurs preferentially at high latitudes, especially when the IMF clock angle is $< 150°$. While inferred high-latitude merging sites favor the antiparallel merging hypothesis, our data alone cannot exclude the possibility of a guide field. Merging can move away the equator even when the IMF has a strong southward component. ISM simulations suggest that this effect is due to tilting of the dipole axis away from the Sun. We also found that IMF B_X affects merging rates by enhancing/diminishing the effective dipole tilt angle. Observations show that high-latitude merging rates can vary temporally with periods of 1–3 min. These variations appear to be directly driven by variations in the interplanetary electric field (Maynard et al., 2001b), or may arise from unstable processes within the magnetosheath/magnetosphere interface.

References

Aggson, T. L., Gambardella, P. J., and Maynard, N. C.: Electric field measurements at rotational magnetopause discontinuities, J. Geophys. Res., 88, 10 000–10 010, 1983.

Aggson, T. L., Maynard, N. C., Ogilvie, K. W., Scudder, J. D., and Gambardella, P. J.: Observations of plasma deceleration at a rotational magnetopause discontinuity, Geophys. Res. Lett., 11, 8–11, 1984.

Atkinson, G.: Mechanism by which merging at X-lines causes discrete auroral arcs, J. Geophys. Res., 97, 1337–1344, 1992.

Balogh, A., Carr, C. M., Acuna, M. H., Dunlop, M. W., Beek, T. J., Brown, P., Fornacon, K.-H., Georgescu, E., Glassmeier, K.-H., Harris, J., Musmann, G., Oddy, T., and Schwingenschuh, K.: The Cluster magnetic field investigation: overview of in-flight performance and initial results, Ann. Geophysicae, 19, 1207–1217, 2001.

Bauer, T. M., Paschmann, G., Sckopke, N., Treumann, R. A., Baumjohann, W., and Phan, T.-D.: Fluid and particle signatures of dayside reconnection, Ann. Geophysicae, 19, 1045–1063, 2001.

Cauffman, D. P. and Maynard, N. C.: A Model of the Effect of the Satellite Photosheath on a Double Floating Probe System, J. Geophys. Res., 79, 2427–2438, 1974.

Coleman, I. J., Chisham, G., Pinnock M., and Freeman, M. P.: An ionospheric convection signature of antiparallel reconnection, J. Geophys. Res., 106, 28 995–29 007, 2001.

Cowley, S. W. H.: The causes of convection in the Earth's magnetosphere: A review of developments during the IMS, Rev. Geophys. Space Phys., 20, 531, 1982.

Cowley, S. W. H. and Lockwood, M.: Excitation and decay of solar wind driven flows in the magnetosphere-ionosphere system, Ann. Geophysicae, 10, 103–115, 1992.

Cowley, S. W. H. and Owen, C. J.: A simple illustrative model of open flux tube motion over the dayside magnetopause, Planet. Space. Sci., 37, 1461, 1989.

Crooker, N. U.: Dayside merging and cusp geometry, J. Geophys. Res., 84, 951–959, 1979.

Crooker, N. U.: Reverse convection, J. Geophys. Res., 97, 19 363–19 372, 1992.

deHoffman, F. and Teller, E.: Magnetohydrodynamic shocks, Phys. Rev., 80, 292, 1950.

Dungey, J. W.: Interplanetary magnetic field and the auroral zones, Phys. Rev. Lett., 6, 47, 1961.

Dunlop, M. W., Balogh, A., Glassmeier, K.-H., and Robert, P.: Four-point Cluster application of magnetic field analysis tools: The curlometer, J. Geophys. Res., 167(A11), 1384, doi:10.1029/2001JA005088, 2002.

Eastman, T. E., Hones, E. W., Jr., Bame, S. J., and Asbridge, J. R.: The magnetospheric boundary layer: Site of plasma, momentum and energy transfer from the magnetosheath into the magnetosphere, Geophys. Res. Lett., 3, 685–688, 1976.

Farrugia, C. J., Dunlop, M. W., Elliott, S., Freeman, M. P., Balogh, A., Cowley, S. W. H., Lepping, R. P., and Sibeck, D. G.: Multipoint observations of planar interplanetary field structures, J. Atmos. Terr. Phys., 53, 1039–1047, 1991.

Farrugia, C. J., Vasquez, B., Richardson, I. G., Torbert, R. B., Burlaga, L. F., Biernat, H. K., Muehlbachler, S., Ogilvie, K. W.,

Lepping, R. P., Scudder, J. D., Berdichevsky, D. E., Semenov, V. S., Kubyshkin, I. V., Phan, T.-D., and Lin, R. P.: A reconnection layer associated with a magnetic cloud, Adv. Space Res., 28(5), 759–764, 2001.

Fuselier, S. A., Klumpar, D. M., and Shelley, E. G.: Ion reflection and transmission during reconnection at the Earth's subsolar magnetopause, Geophys. Res. Lett., 18, 139–142, 1991.

Gonzalez, W. D. and Mozer, F. S.: A quantitative model for the potential resulting from reconnection with arbitrary interplanetary magnetic field, J. Geophys. Res., 79, 4186, 1974.

Gosling, J. T., Asbridge, J. R., Bame, S. J., Feldman, W. C., Paschmann, G., Sckopke, N., and Russell, C. T.: Evidence for quasi-stationary reconnection at the dayside magnetopause, J. Geophys. Res., 87, 2147, 1982.

Greenwald, R. A., Baker, K. B., Dudeney, J. R., Pinnock, M., Jones, T. B., Thomas, E. C., Villain, J. P., Cresier, J. C., Senior, C., Hanuise, C., Hunsucker, R. D., Sofko, G., Koehler, J., Nielsen, E., Pallinen. R., Walker, A. D. M., Sato, N., and Yamagishi, H.: DARN and SuperDARN: A global view of high-latitude convection, Space Sci. Rev., 71, 761–796, 1995.

Gustafsson, G., Boström, R., Holback, B., Holmgren, G., Lundgren, A., Stasiewicw, K., Åhlèn, L., Mozer, F. S., Pankow, D., Harvey, P., Ulrich, R., Pedersen, A., Schmidt, R., Butler, A., Fransen, A. W. C., Klinge, D., Thomsen, M., Fälthammar, C.-G., Lindqvist, P.-A., Christenson, S., Holtet, J., Lybekk, B., Sten, T. A., Tanskenen, P., Lappalainen, K., and Wygant, J.: The electric field and wave experiment for the Cluster mission, Space Sci. Rev., 79, 137–156, 1997.

Hain, K.: The partial donor cell method, J. Comp. Physics, 73, 131, 1987.

Harvey, P., Mozer, F. S., Pankow, D., Wygant, J., Maynard, N. C., Singer, H., Sullivan, W., Anderson, P. B., Pfaff, R., Aggson, T., Pedersen, A., Fälthammar, C.-G., and Tanskannen. P.: The electric field instrument on the Polar satellite, Space Sci. Rev., 71, 583–596, 1995.

Kim, K.-H., Lin, N., Cattell, C. A., Song, Y., and Lee, D.-H.: Evidence for component merging near the subsolar magnetopause: Geotail observations, Geophys. Res. Lett., 29, 10.1029/2001GL014636, 2002.

Lee, L. L. and Kan, J. R.: A unified kinetic model of tangential magnetopause structure, J. Geophys. Res., 84, 6417, 1979.

Lepping, R. P., Acuña, M. H., Burlaga, L. F., Farrell, W. M., Slavin, J. A., Schatten, K. H., Mariani, F., Ness, N. F., Neubauer, F. M., Whang, Y. C., Byrnes, J. B., Kennon, R. S., Panetta, P. V., Schiefele, J., and Worley, E. M.: The Wind magnetic field Investigation, Space Sci. Rev., 71, 207–229, 1995.

Levy, R. H., Petschek, H. E., and Siscoe, G. L.: Aerodynamic aspects of magnetospheric flow, AIAA J., 2, 2065, 1964.

Ma, Z. W. and Bhattacharjee, A.: Hall magnetohydrodynamic reconnection: The Geospace Environment Modeling challenge, J. Geophys. Res., 106, 3773–3782, 2001.

Maynard, N. C., Burke, W. J., Basinska, E. M., Erickson, G. M., Hughes, W. J., Singer, H. J., Yahnin, A. G., Hardy, D. A., and Mozer, F. S.: Dynamics of the inner magnetosphere near times of substorm onsets, J. Geophys. Res., 101, 7705–7736, 1996a.

Maynard, N. C., Burke, W. J., Erickson, G. M., Basinska, E. M., and Yahnin, A. G.: Magnetosphere-ionosphere coupling during substorm onset, in Third International Conference on Substorms (ICS-3), ESA SP389, 301–305, ESA Publications Div., Noordwijk, The Netherlands, 1996b.

Maynard, N. C., Weber, E. J., Weimer, D. R., Moen, J., Onsager, T., Heelis, R. A., and Egeland, A.: How wide in magnetic local time

is the cusp?: An event study, J. Geophys. Res., 102, 4765–4776, 1997.

Maynard, N. C., Burke, W. J., Pfaff, R. F., Weber, E. J., Ober, D. M., Weimer, D. R., Moen, J., Milan, S., Sandholt, P. E., Egeland, A., Søraas. F., Lepping, R., Bounds, S., Acuña, M. H., Freudenreich, H., Gentile, L. C., Hardy, D. A., Holtet, J. A., Lester, M., Machuzak, J. S., Clemmons, J. H., Ning, P., Stadsnes, J., and van Eyken, T.: Driving dayside convection with northward IMF: Observations by a sounding rocket launched from Svalbard, J. Geophys. Res., 105, 5245–5263, 2000.

Maynard, N. C., Savin, S., Erickson, G. M., Kawano, H., Némeçek, Z., Peterson, W. K., Šafrànokovà, J., Sandahl, I., Scudder, J. D., Siscoe, G. L., Sonnerup, B. U. Ö., Weimer, D. R., White, W. W., and Wilson, G. R.: Observation of the magnetospheric "sash" and its implications relative to solar-wind/magnetospheric coupling: A multisatellite event analysis, J. Geophys. Res., 106, 6097–6122, 2001a.

Maynard, N. C., Burke, W. J., Sandholt, P. E., Moen, J., Ober, D. M., Lester, M., Weimer, D. R., and Egeland, A.: Observations of simultaneous effects of merging in both hemispheres, J. Geophys. Res., 106, 24 551–24577, 2001b.

Maynard, N. C., Burke, W. J., Moen, J., Ober, D. M., Scudder, J. D., Sigwarth, J. B., Siscoe, G. L., Sonnerup, B. U. Ö., White, W. W., Siebert, K. D., Weimer, D. R., Erickson, G. M., Frank, L. A., Lester, M., Peterson, W. K., Russell, C. T., Wilson, G. R., and Egeland, A.: Responses of the open-closed field line boundary in the evening sector to IMF changes: A source mechanism for Sun-aligned arcs, J. Geophys. Res., 108(A1), 1006, doi10.129/2001JA000174, 2003a.

Maynard, N. C., Burke, W. J., Scudder, J. D., Ober, D. M., Siscoe, G. L., White, W. W., Siebert, K. D., Weimer, D. R., Erickson, G. M., Schoendorf, J., Wilson, G. R., and Heinemann, M. A.: Observed and simulated depletion layers with southward IMF, submitted to Annales Geophysicae, 2003b.

McComas, D. J., Bame, S. J., Barber, P., Fieldman, W. C., Phillips, J. L., and Riley, P.: Solar wind electron, proton, and alpha monitor (SWEPAM) on the Advanced Composition Explorer, Space Sci. Rev., 86, 563–612, 1998.

Moore, T. E., Fok, M.-C., and Chandler, M. O.: The dayside reconnection X-line, J. Geophys. Res., 107(A10), 1332, doi:10.129/2001JA000049, 2002.

Mozer, F. S., Bale, S. D., and Phan, T. D.: Evidence of Diffusion Regions at a Subsolar Magnetopause Crossing, Phys. Rev. Lett., 89, no. 1, 015002, 2002.

Nakamura, M., Seki, K., Kawano, H., Obara, T., and Mukai, T.: Reconnection event at the dayside magnetopause on January 10, 1997, Geophys. Res. Lett., 25, 2529, 1998.

Ogilvie, K. W., Chornay, D. J., Fritzenreiter, R. J., Hunsaker, F., Keller, J., Lobell, G, Miller, G., Scudder, J. D., Sittler, Jr., E. C., Torbert, R. B., Bodet, D., Needell, G., Lazarus, A. J., Steinberg, J. T., Tappan, J. H., Mavretic, A., and Gergin, E.: SWE: A comprehensive plasma instrument for the wind spacecraft: Space Sci. rev., 71, 55–77, 1995.

Paschmann, G., Sonnerup, B. U. Ö, Papamastorakis, I., Sckopke, N., Haerendel, G., Bame, S. J., Asbridge, J. R., Gosling, J. T., Russell, C. T., and Elphic. R. C.: Plasma acceleration at the earth's magnetopause: Evidence for reconnection, Nature, 282, 243–246, 1979.

Paschmann, G., Papamastorakis, I., Baumjohann, W., Sckopke, N., Sonnerup, B. U. Ö., and Lühr, H.: The magnetopause for large magnetic shear: AMPTE/IRM observations, J. Geophys. Res., 91, 11 099–11 115, 1986.

Phan, T.-D., Paschmann, G., and Sonnerup, B. U. Ö.: Low latitude dayside magnetopause and boundary layer for high magnetic shear: 2. Occurrence of magnetic reconnection, J. Geophys. Res., 101, 7817, 1996.

Phan, T. D., Kistler, L. M., Klecker, B., Haerendel, G., Paschmann, G., Sonnerup, B. U. Ö., Baumjohann, W., Bavassano-Cattaneo, M. B., Carlson, C. W., DiLellis, A. M., Fornacon, K. -H., Frank, L. A., Fujimoto, M., Georgescu, E., Kokubun, S., Moebius, E., Mukai, T., Øieroset, M., Paterson, W. R., and Rème, H.: Extended magnetic reconnection at the Earth's magnetopause from detection of bi-directional jets, Nature, 404, 848–850, 2000.

Rème, H., Bosqued, J. M., Sauvaud, J. A., Cros, A., Dandouras, J., Aoustin, C., Bouyssou, C., Camus, Th., Cuvilo, J., Martz, C., Medale, J. L., Perrier, H., Romefort, D., Rouzaud, J., dUston, C., Möbius, E., Crocker, K., Granoff, M., Kistler, L. M., Popecki, M., Hovestadt, D., Klecker, B., Paschmann, G., Scholer, M., Carlson, C. W., Curtis, D. W., Lin, R. P., McFadden, J. P., Formisano, V., Amata, E., Bavassano-Cattaneo, M. B., Baldetti, P., Belluci, G., Bruno, R., Chionchio, G., DiLellis, A., Shelley, A. G., Ghielmetti, A. G., Lennartsson, W., Korth, A., Rosenbauer, H., Lundin, R., Olsen, S., Parks, G. K., McCarthy, M., and Balsiger, H.: The Cluster ion spectrometry (CIS) experiment, Space Sci. Rev., 79, 303–350, 1997.

Rodger, A. S., Coleman, I. J., and Pinnock, M.: Some comments on transient and steady-state reconnection at the dayside magnetopause, Geophys. Res. Lett., 27, 1359–1362, 2000.

Ruohoniemi, J. M. and Baker, K. B.: Large-scale imaging of high-latitude convection with Super Dual Aurora Radar network HF radar observations, J. Geophys. Res., 103, 20 797–20811, 1998.

Ruohoniemi, J. M. and Greenwald, R. A.: Statistical patterns of high-latitude convection obtained from Goose Bay HF radar observations, J. Geophys. Res., 101, 21 746–21 763, 1996.

Russell, C. T., Snare, R. C., Means, J. D., Pierce, D., Dearborn, D., Larson, M., Barr, G., and Le, G.: The GGS/polar magnetic field investigation, Space Sci. Rev., 71, 563–582, 1995.

Scudder, J. D.: Fluid signatures of rotational discontinuities, J. Geophys. Res., 89, 7431–7440, 1984.

Scudder, J. D., Hunsaker, F., Miller, G., Lobell, J., Zawistowski, T., Ogilvie, K., Keller, J., Chornay, D., Herrero, F., Fitzenreiter, R., Fairfield, D., Needell, J., Bodet, D., Googins, J., Kletzing, C., Torbert, R., Vandiver, J., Bentley, R., Fillius, W., McIlwain, C., Whipple, E., and Korth, A.: Hydra: A three dimensional electron and ion instrument for the polar spacecraft of the GGS mission, Space Sci. Rev., 71, 459–495, 1995.

Scudder, J. D., Puhl-Quinn, P. A., Mozer, F. S., Ogilvie, K. W., and Russell, C. T.: Generalized Walén tests through Alfvén waves and rotational discontinuities using electron velocities, J. Geophys. Res., 104, 19 817–19 833, 1999.

Scudder, J. D., Mozer, F. S., Maynard, N. C., and Russell, C. T.: Fingerprints of collisionless reconnection at the separator: I, Ambipolar-Hall signatures, J. Geophys. Res., 107(A10), 1294, 10.1029/2001JA000126, 2002a.

Scudder, J. D., Maynard, N., Ober, D., and Mozer, F.: Ambipolar electric fields parallel and perpendicular to the local magnetic field: Magnetopause and depletion layers, SM21C-04, Fall meeting of the AGU, 2002b.

Scurry, L., Russell, C. T., and Gosling, J. T.: A statistical study of accelerated flow events at the dayside magnetopause, J. Geophys. Res., 99, 14 815–14 829, 1994.

Siscoe, G. L.: Solar system magnetohydrodynamics, in: Solar Terrestrial Physics, edited by R. L. Carovillano and J. Forbes, Reidel, D. Publishing Co., Hingham, MA, 11–100, 1983.

Siscoe, G. L., Erickson, G. M., Sonnerup, B. U. Ö., Maynard, N. C., Siebert, K. D., Weimer, D. R., and White, W. W.: Deflected magnetosheath flow at high-latitude magnetopause, J. Geophys. Res., 105, 12 851–12 857, 2000.

Siscoe, G. J., Erickson, G. M., Sonnerup, B. U. Ö., Maynard, N. C., Schoendorf, J. A., Siebert, K. D., Weimer, D. R., White, W. W., and Wilson, G. R.: Hill model of transpolar potential saturation: Comparisons with MHD simulations, J. Geophys. Res., 107(A6), 1075, doi: 1029/2001JA00109, 2002a.

Siscoe, G. L., Erickson, G. M., Sonnerup, B. U. Ö., Maynard, N. C., Schoendorf, J. A., Siebert, K. D., Weimer, D. R., White, W. W., and Wilson, G. R.: MHD properties of magnetosheath flow, Planet. Space Sci., 50, 461–471, 2002b.

Smith, C. W., Acuna, M. H., Burlaga, L. F., L'Heureux, J., Ness N. F., and Scheifele, J.: The ACE Magnetic Field Experiment, Space Sci. Rev., 86, 613, 1998.

Song, P., Russell, C. T., and Thomsen, M. F.: Slow mode transition in the frontside magnetosheath, J. Geophys. Res., 97, 8295–8305, 1992.

Sonnerup, B. U. Ö. and Ledley, B. G.: Magnetopause rotational forms, J. Geophys. Res., 79, 4309, 1974.

Sonnerup, B. U. Ö. and Wang, D.-J., Structure of reconnection boundary layers in incompressible MHD, J. Geophys. Res., 92, 8621–8633, 1987.

Sonnerup, B. U. Ö., Paschmann, G., Papamastorakis, I., Sckopke, N., Haerendel, G., Bame, S. J., Asbridge, J. R., Gosling, J. T., and Russell, C. T.: Evidence for magnetic reconnection at the earth's magnetopause, J. Geophys. Res., 86, 10 049, 1981.

Sonnerup, B. U. Ö., Papamastorakis, I., Paschmann, G., and Lühr, H.: The magnetopause for high magnetic shear: Analysis of convection electric fields from AMPTE/IRM, J. Geophys. Res., 95, 10 451–10 557, 1990.

Weimer, D. R., Ober, D., Maynard, N. C., Burke, W. J., Collier, M. R., McComas, D. J., Ness, N. F., and Smith, C. W.: Variable time delays in the propagation of the interplanetary magnetic field, J. Geophys. Res., 107(A8),1210, doi:10.1029/2001JA009102, 2002.

White, W. W., Siscoe, G. L., Erickson, G. M., Kaymaz, Z., Maynard, N. C., Siebert, K. D., Sonnerup, B. U. Ö., and Weimer, D. R.: The magnetospheric sash and cross-tail S, Geophys. Res. Lett., 25, 1605–1608, 1998.

White, W. W., Schoendorf, J. A., Siebert, K. D., Maynard, N. C., Weimer, D. R., Wilson, G. L., Sonnerup, B. U. Ö., Siscoe, G. L., and Erickson, G. M.: MHD simulation of magnetospheric transport at the mesoscale, in: Space Weather, Geophysical Monograph Series Vol. 125, edited by Paul Song, Howard J. Singer, and George L. Siscoe, American Geophys. Union, 229–240, 2001.

Wing, S., Newell, P. T., and Ruohoniemi, J. M.: Double cusp: model prediction and observational verification, J. Geophys. Res., 106, 25 571–25 593, 2001.

Zwan, B. J. and Wolf, R. A.: Depletion of solar wind plasma near a planetary boundary, J. Geophys. Res., 81, 1636–1648, 1976.